34. Pelant, I., Hála, J., Ambrož, M., and Kohlová, V. (1988). *Quantitative analysis of low concentrations of boron and phosphorus in silicon by the laser luminescence spectroscopy—experimental aspects* (In Czech: *Kvantitativní analýza nízkých koncentrací boru a fosforu v křemíku laserovou luminiscenční spektroskopií – experimentální aspekty*). In *Lasers in Research and Industry* (6th Czechoslovak Conference), p. 252. Račkova dolina, SVŠT ČSSP Liptovský Mikuláš.
35. Kaminskii, A. S., Kolesnik, L. I., Leiferov, B. M., and Pokrovskii, Ya. E. (1982). *J. Appl. Spectros.*, **36**, 516.
36. Schumacher, K. L. and Whitney, R. L. (1989). *J. Electron. Mater.*, **18**, 681.
37. Broussell, I., Stolz, J. A. H., and Thewalt, M. L. W. (2002). *J. Appl. Phys.*, **92**, 5913.
38. Zimmermann, H., Boyn, R., Michel, C., and Rudolph, P. (1990). *phys. stat. sol. (a)*, **118**, 225.
39. Thewalt, M. L. W., Nissen, M. K., Beckett, D. J. S., and Lungren, K. R. (1989). *High-performance photoluminescence spectroscopy using Fourier-transform interferometry*, MRS Meeting Boston November/December, Symp. G. *MRS Symposium Proceedings*, **163**, (1990), 221.
40. Dekker, A. J. (1963). *Solid State Physics*. Prentice-Hall, Englewood Cliffs, N.J.; Curie, D. (1960). *Luminescence Cristalline*. Dunod, Paris.
41. Gershoni, D., Cohen, E., and Ron, A. (1985). *J. Luminescence*, **34**, 83.
42. Pelant, I. (1988). *Laser luminescence spectroscopy of some crystalline semiconductors and ionic crystals* (In Czech: *Laserová luminiscenční spektroskopie vybraných krystalických polovodičů a dielektrik*), DSc Thesis, Charles University in Prague, Faculty of Mathematics and Physics, Prague.
43. Tsukakoshi, M. and Kanzaki, H. (1971). *J. Phys. Soc. Japan*, **30**, 1423.
44. Stolz, H., von der Osten, W., and Weber, J. (1976). *Lifetime and time-resolved spectra of indirect excitons in AgBr*. In *Physics of Semiconductors* (ed. F. G. Fumi), p. 865. *Proceedings of the 13th International Conference on the Physics of Semiconductors*, Rome.
45. Holonyak, N. Jr., Campbell, J. C., Lee, M. H., Verdeyen, J. T., Johnson, W. L., Craford, M. G., and Finn, D. (1973). *J. Appl. Phys.*, **44**, 5517.
46. Vishnevskaya, B. I., Korneev, V. M., Kogan, L. M., and Yunovich, A. E. (1973). *Soviet Phys. Semicond.*, **6**, 1372.
47. Craford, M. G. and Holonyak, N. Jr. (1976). *The optical properties of the nitrogen isoelectronic trap in $GaAs_{1-x}P_x$*. In *Optical Properties of Solids. New Developments* (ed. B. O. Seraphin), p. 187. North Holland, Amsterdam.
48. Brown, T. G. and Hall, D. G. (1998). *Radiative isoelectronic impurities in silicon and silicon–germanium alloys*. In *Light Emission in Silicon: From Physics to Devices* (ed. D. J. Lockwood), *Semiconductors and Semimetals* Vol. 49, p. 77. Academic Press, San Diego.
49. Toyozawa, Y. (1970). *J. Luminescence*, **1**, 632; Toyozawa, Y. (1981). *J. Luminescence*, **24/25**, 23.
50. Kobayashi, M., Matsushima, Y., Nishi, O., Mizuno, K., and Matsui, A. H. (1995). *SPIE*, **2362** (*Exciton processes in condensed matter*), 225.
51. von der Osten, W. (1984). *Excitons and exciton relaxation in silver halides*. In *Polarons and Excitons in Polar Semiconductors and Ionic Crystals* (ed. J. T Devreese and F. Peeters), p. 293. Plenum Press, New York.
52. Pelant, I. and Hála, J. (1991). *Solid State Comm.*, **78**, 141.
53. Nakagawa, H., Muneda, Y., and Matsumoto, H. (1988). *J. Luminescence*, **40/41**, 485.
54. Lee, D., Mysyrowicz, A., Nurmikko, A. V., and Fitzpatrick, B. J. (1987). *Phys. Rev. Lett.*, **58**, 1475.
55. Song, K. S. and Williams, R. T. (1996). *Self-Trapped Excitons*. Springer Series in Solid State Sciences Vol. 105. Springer, Berlin.
56. Zhao, H. and Kalt, H. (2003). *Phys. Rev. B*, **68**, 12.

Highly excited semiconductors

8

The channels of radiative recombination, discussed in Chapters 5 and 7, are characteristic of conventional (weak) optical excitation when the excitation power densities on the sample surface amount to 0.01–10 W/cm^2. When the excitation intensity is increased to kW/cm^2–MW/cm^2 (which is attainable almost exclusively with the aid of pulsed lasers) the emission spectrum undergoes substantial modifications: New emission lines or bands appear. Figure 8.1 shows a typical example [1]. These lines or bands signify novel luminescence processes occurring in highly excited semiconductors, in particular: radiative decay of excitonic molecules (biexcitons), collisions between excitons, luminescence of the electron–hole liquid or electron–hole plasma and Bose–Einstein condensation of excitons or biexcitons. We are going to discuss these

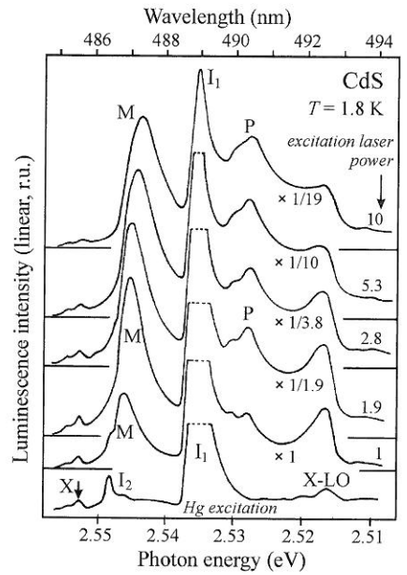

Fig. 8.1
Edge emission spectrum of CdS under various intensities of optical excitation (temperature $T = 1.8$ K). The lowermost spectrum was acquired at a conventional Hg-lamp excitation ($\lambda_{ex} = 365$ nm) and is dominated by I_1 and I_2 lines, which are due to excitons bound to residual impurities. The X-line belongs to the resonant emission of an exciton–polariton (compare with Fig. 7.11(a)). The remaining spectra were excited by a pulsed N_2-laser ($\lambda_{ex} = 337$ nm), relative excitation power densities being indicated to the right along with normalization factors. The figure illustrates that the I_1, I_2 lines gradually saturate with increasing excitation intensity while novel M and P lines appear. After Shionoya *et al.* [1].

phenomena in the present chapter. Optical properties of highly excited semiconductors are dealt with also, e.g. in special issues of *Physics Reports* [2, 3].

8.1 Experimental considerations

To understand the underlying physical nature of the novel luminescence processes occuring under high excitation, it appears advantageous to characterize the concentration level of created free excitons n_X. We can start with eqn (3.4) from which it follows that in steady-state conditions

$$n_X \cong I_{ex}\,\alpha\,\tau, \tag{8.1}$$

where I_{ex} stands for the excitation photon flux (photon/cm^{2}s) of energy $h\nu_{ex}$, α(cm^{-1}) denotes the absorption coefficient at energy $h\nu_{ex}$ and τ (s) means the exciton lifetime. For a typical case of band $\rightarrow$ band excitation we consider $\alpha \cong 10^5$cm^{-1}, $\tau = 10^{-9}$s (direct semiconductor) and the excitation photon flux I_{ex} can be derived from the excitation intensity P_{ex}—usually expressed in watts per cm^2—using the relation $I_{ex} = (P_{ex}/h\nu_{ex})$. For $P_{ex} = 1\,\mathrm{W/cm^2}$ (conventional weak excitation) and $h\nu_{ex} = 3$ eV we have $I_{ex} \cong 2 \times 10^{18}$ photon/cm^2 s and the density of photogenerated excitons (8.1) becomes $n_X \cong 2 \times 10^{14}\,\mathrm{cm^{-3}}$.

Given $\ell_X \cong \sqrt[3]{(1/n_X)}$) as the mean interexciton separation, we get in this case $\ell_X \cong 170$ nm. Comparing this value with a typical exciton Bohr radius $a_X \cong 5$ nm (Table 7.1) implies $\ell_X \gg a_X$, and therefore free excitons are sufficiently separated from each other and do not enter into interactions. However, if we increase their density so that ℓ_X approaches the exciton diameter $2a_X$, the situation becomes completely different. The condition $\ell_X \cong 2a_X$ yields (keeping $a_X = 5$ nm) the exciton density $n_X \cong 10^{18}\,\mathrm{cm^{-3}}$ and the corresponding excitation photon flux is, using (8.1), equal to $I_{ex} \approx 10^{22}$ photon/cm^2 s or, equivalently, to the excitation intensity $P_{ex} = I_{ex}h\nu_{ex} \approx 5\,\mathrm{kW/cm^2}$.[1]

At such excitation intensities one can already expect the occurence of interactions between excitons. These, as we shall see, may dramatically modify the luminescence behaviour of the material under study. It is worth stressing, however, that relation (8.1) is not exact; the density of excitons or electron–hole pairs under standard one-photon excitation is considerably inhomogeneous. The concentration gradient pushes them from a thin subsurface layer with thickness $\alpha^{-1} < 1\,\mu$m deeper into the sample, thereby rapidly reducing their concentration. Besides, excitons close beneath the surface undergo efficient surface non-radiative recombination (Fig. 6.2). That is why the excitation intensities P_{ex} applied in experiments must in fact be higher than the above order-of-magnitude estimate—they usually range from $\sim 1\,\mathrm{kW/cm^2}$ up to 1–10 MW/cm^2, where the upper bound is driven by the threshold of mechanical destruction of the sample by powerful laser pulses.

[1] For expressing the density of excitons or electron–hole pairs, one sometimes exploits the dimensionless parameter $r_s = (3/4\pi n_X)^{1/3}(1/a_X)$; high densities n_X are characterized by values $r_s < 1$.

Two remarks may be in order. The first one refers to most indirect-bandgap semiconductors (Si, Ge, GaP). Here, the exciton lifetime is much longer than 10^{-9} s and high exciton densities $r_s < 1$ can already be achieved using cw lasers or even conventional high-pressure lamps.

The second remark points to the principal superiority of two-photon excitation for studying luminescence of high-density excitonic systems. Owing to the very slow decrease of excitation intensity along the penetration depth inside the sample (Fig. 5.15(a)), relation (8.1) holds—contrary to the one-photon case—very accurately. We can thus achieve a pre-determined value of homogeneous exciton concentration over the whole volume of the sample, which is highly desirable for comparing the experimentally deduced density with various models of excitonic interactions discussed below. Of course, we have to replace the one-photon absorption coefficient α in (8.1) by its two-photon analogue $\alpha^{(2)}$, defined in the context of eqn (5.22) as

$$\alpha^{(2)} = aI_0 = aP_{ex}(\mathrm{cm^{-1}}) \tag{8.2}$$

(that is, we denote the excitation power density as P_{ex} in this chapter). The reader is reminded that a is a material constant with a typical value of $a \cong 10^{-3}$ cm/MW.

However, there is one hitch in this, namely, if we realize how low the amount of energy deposited generally into the electronic system of the sample under two-photon excitation is. Introducing $\alpha^{(2)}$ from (8.2) to (8.1) and expressing P_{ex} as a function of the required exciton concentration, we get

$$P_{ex} = \sqrt{n_X\, h\, \nu_{ex}/\tau\, a}. \tag{8.3}$$

Therefore, if we wish to generate a homogeneous exciton concentration $n_X = 10^{17}\,\mathrm{cm^{-3}}$, using typical values of $h\nu_{ex} = 3\,\mathrm{eV} \approx 5 \times 10^{-19}$ J, $\tau = 10^{-9}$ s and $a = 10^{-3}$ cm/MW, it follows from (8.3) that the required excitation power density P_{ex} reaches $\sim 100\,\mathrm{MW/cm^2}$! Such a high value of excitation power density is already comparable with the threshold of sample destruction. We have to carefully look up all possible material parameters (especially the value of a) in advance, as well as evaluate all the capabilities of our experimental set-up. Only then can we decide whether the possible advantage of achieving a homogeneous density of exciton gas would not be nullified by damaging the sample.

8.2 Excitonic molecule or biexciton

Referring to the similarity between a free exciton and a hydrogen atom, discussed in Section 7.1, we can expect that with increasing free exciton density a 'fusion' of two excitons into an excitonic molecule (EM) or biexciton will occur, in analogy with the fusion of two hydrogen atoms into a hydrogen molecule. An EM is a quasi-particle consisting of two electrons and two holes and propagating freely through the crystal lattice (more exactly, we should designate it as a *free biexciton*). It is obvious that the very existence of EMs in a given semiconductor will be critically dependent upon the ratio of the electron and hole effective masses $\sigma = m_e/m_h$, much like as in bound exciton

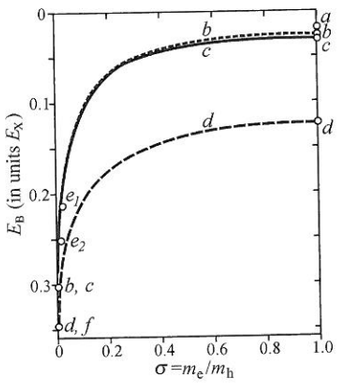

Fig. 8.2
Examples of theoretically calculated dependencies of the biexciton binding energy E_B upon the ratio of the electron and hole effective masses $\sigma = m_e/m_h$. E_B is expressed in units of the free exciton binding energy E_X. Small letters denote results obtained by different authors. Adapted from Quattropani and Forney [4], where the reader can find a more detailed discussion.

complexes discussed in Subsection 7.2.1. Both an electron and a hole are very light quasi-particles and thus the resulting large amplitude of biexciton zero-point vibrations will have a tendency to dissociate the excitonic molecule even at low temperatures. The measure of EM stability against dissociation into two free excitons is its binding energie E_B.

Theoretical calculations of E_B using diverse variation methods have been performed by many authors; the results, as compiled by Quattropani and Forney, are depicted in Fig. 8.2 [4]. It is observed that an EM is a stable entity ($E_M \geq 0$) for an arbitrary value of σ, even if, quite naturally, the binding energy strongly increases in the case of heavy holes.

It is important to note that the calculations predict, for typical values of σ in semiconductors ($\sigma \approx 0.1$–0.5), that the magnitude of the binding energy E_B will be approximately equal to one-tenth of the free exciton binding energy: $E_B \cong 0.1 E_X$. A biexciton is therefore substantially less resistant to thermal dissociation than an exciton. An important message for experiments is that for studying biexcitons very low temperatures are required in most cases (about 1.3–50 K), accessible in liquid helium cryostats only.

Radiative recombination of EMs is a process in which one of the excitons forming the molecule undergoes a transition to the free exciton $n = 1$ state while the second one recombines, emitting a photon $h\nu_M$. This process gives rise to a novel emission line (e.g. the M-line in Fig. 8.1). In order to be able to assign reliably an experimentally observed line to excitonic molecule decay, we have to analyse its lineshape, intensity dependence, spectral position and temperature behaviour.

8.2.1 Identification of the EM emission line

The basic guideline for the indentification of an emission line as being due to radiative decay of an EM is its characteristic lineshape. It turns out to be suitable to discuss the EM emission lineshape separately in direct-bandgap and indirect-bandgap semiconductors.

Luminescence of excitonic molecule in a direct semiconductor

To begin, we determine the approximate spectral position of the EM emission line, neglecting the kinetic energies of all participating quasi-particles.

The formation of an EM through the 'fusion' of two excitons with energies (E_g–E_X), accompanied by a simultaneous release of binding energy E_B, leads to a biexciton in its ground state with an energy of $2(E_g$–$E_X)$–E_B (see Fig. 8.3(a)). Radiative decay of the biexciton generates one photon, $h\nu_M$, and leaves behind one free exciton, therefore the total energy of the system reads $h\nu_M + (E_g$–$E_X)$. Comparing the above mentioned energies yields the overall energy balance

$$2(E_g - E_X) - E_B = h\nu_M + (E_g - E_X) \tag{8.4}$$

or

$$h\nu_M = (E_g - E_X) - E_B. \tag{8.5}$$

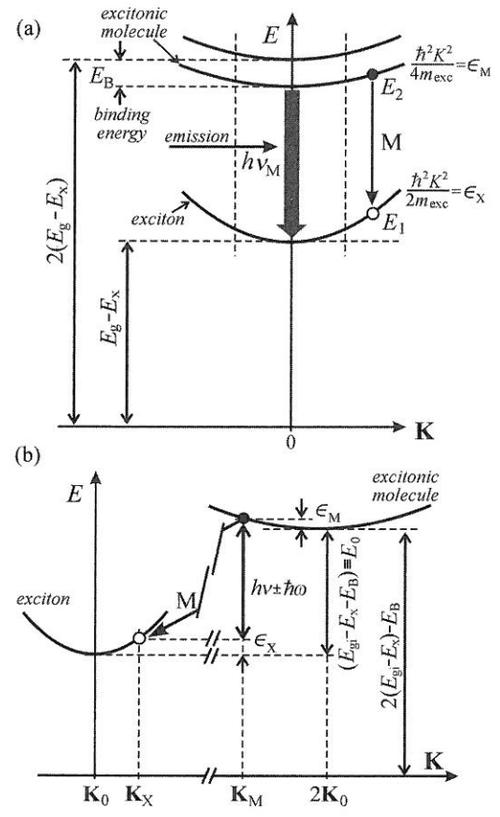

Fig. 8.3
Radiative decay of an excitonic molecule in an $E(\mathbf{K})$ diagram for (a) a direct-bandgap semiconductor and (b) an indirect-bandgap semiconductor with the indirect bandgap situated at $\mathbf{K}_0$. The scheme goes, of course, beyond the limit of the one-electron approximation (otherwise the energy level of the excitonic molecule would be 'submerged' high up into the conduction band).

Hence, the emission line of the EM is shifted with respect to the position of the free exciton absorption line (E_g–E_X) (or the luminescence line of an exciton–polariton) by the binding energy E_B towards low photon energies.

Now we take into consideration also the kinetic energies in the ensemble of excitonic molecules and free excitons. We shall arrive at important information on the characteristic biexciton spontaneous emission lineshape $I_{sp}^{M}(h\nu)$, namely, that it is of a mirror-like appearance with regard to the free exciton emission lineshape described by expressions (7.13) or (7.16). We speak of the inverse Maxwell–Boltzmann distribution (with effective temperature T_M of the biexciton gas), i.e.

$$I_{sp}^{M}(h\nu) \cong [(E_g - E_X - E_B) - h\nu]^{1/2} \exp\{-[(E_g - E_X - E_B) - h\nu]/k_B T_M\}. \tag{8.6}$$

Prior to deriving expression (8.6) rigorously, we shall attempt to understand this lineshape qualitatively employing Fig. 8.3(a). The biexciton dispersion curve $\epsilon_M(\mathbf{K}) = h^2K^2/4m_{exc}$ (where $m_{exc} = m_e + m_h$ is the exciton mass) is less curved compared with the exciton curve $\epsilon_X(\mathbf{K}) = h^2K^2/2m_{exc}$. The highest emitted photon energy thus belongs to the downward transition at $\mathbf{K} = |0\rangle$ and is, according to (8.5), equal to $(E_g$–$E_X)$–E_B; radiative decay of

biexcitons with non-zero kinetic energy at $\mathbf{K} \neq |0\rangle$ results in luminescence photons with lower energy, which is depicted in Fig. 8.3(a) by the transition M between states E_2 and E_1. Therefore, the emission line will have an asymmetric shape characterized by a high-energy edge at $(E_g–E_X)–E_B$ followed by a low-energy tail.

To derive (8.6) we shall apply a procedure similar to that utilized in Subsection 5.2.1 for deducing the Maxwell–Boltzmann distribution (5.9a). Spontaneous emission of a luminescence photon pertaining to radiative decay of a biexciton $I_{sp}^{M}(h\nu)$ is driven by (i) the optical joint density of states $\rho_M(h\nu)$, coming from the relevant densities of states in the exciton and biexciton bands,[2] (ii) the population fraction $f_M(h\nu)$ of the biexciton states and (iii) the transition matrix element M_M:

$$I_{sp}^{M}(h\nu) \sim \rho_M(h\nu) f_M(h\nu) |M_M|^2. \tag{8.7}$$

The matrix element M_M is considered to be independent of $h\nu$. Referring to Fig. 8.3(a) we can write

$$E_2 = 2(E_g - E_X) - E_B + \hbar^2 K^2/4\, m_{exc}, \tag{8.8a}$$

$$E_1 = (E_g - E_X) + \hbar^2 K^2/2\, m_{exc}, \tag{8.8b}$$

which immediately implies

$$h\nu = E_2 - E_1 = (E_g - E_X - E_B) - \hbar^2 K^2/4\, m_{exc}, \tag{8.8c}$$

hence

$$K^2 = \frac{4\, m_{exc}}{\hbar^2}[(E_g - E_X - E_B) - h\nu]. \tag{8.9}$$

Inserting for K^2 from (8.9) to (8.8b) yields

$$E_1 = 2[(E_g - E_X - E_B) - h\nu] + (E_g - E_X). \tag{8.10}$$

Let us suppose now that the density of states in the exciton band ρ_X has the common square-root form, fully analogous to the densities of states in the conduction and valence bands, expressed by formula (5.4):

$$\rho_X(E_1) = \frac{(2\, m_{exc})^{2/3}}{2\,\pi^2\,\hbar^3} \sqrt{E_1 - (E_g - E_X)}. \tag{8.11}$$

By using the incremental relation

$$\rho_X(E_1)\, \mathrm{d}E_1 = -\rho_M(h\nu)\, \mathrm{d}(h\nu)$$

(the '–' sign means here that the loss of one free exciton state is equivalent to the generation of one photon $h\nu$) along with (8.10) and (8.11) we find the optical joint density of states

$$\rho_M(h\nu) = -\rho_X(E_1)\, \mathrm{d}E_1/\mathrm{d}(h\nu) = -\rho_X(E_1)(-2)$$
$$= \frac{\sqrt{2}(2m_{exc})^{3/2}}{\pi^2\,\hbar^3} \sqrt{(E_g - E_X - E_B) - h\nu}. \tag{8.12}$$

[2] The reader is reminded that the possibilty of introducing the joint density of states follows from the verticality of the transitions depicted in Fig. 8.3(a).

Finally, the population factor $f_M(h\nu)$ in (8.7) can be determined quite easily: Since both biexcitons and excitons are composed of an even number of fermions, they have integer spin and are, therefore, bosons. Then, there is no need—contrary to direct interband e–h transitions—to formulate any mathematical condition concerning the occupancy of the exciton dispersion curve; the population fraction is driven exclusively by the occupation probability of the upper (biexciton) level. This is given by the Boltzmann factor

$$f_M(h\nu) \approx \exp(-\hbar^2 K^2/4\, m_{exc}\, k_B T_M)$$
$$= \exp\left[-(E_g - E_X - E_B - h\nu)/k_B T_M\right].$$

By combining this expression with (8.12) we obtain, according to (8.7), the emission lineshape of biexciton luminescence (8.6).

The reader will have certainly noticed that the above considerations were conducted under the tacit assumption of the validity of not only energy conservation, but also quasi-momentum conservation for the whole recombining biexciton population. In other words, all biexcitons are supposed to take part in the radiative decay, independently of the magnitude of their wavevector $\mathbf{K}$. This represents a fundamental difference from the free exciton luminescence in direct-bandgap materials, where the radiative recombination can occur only for $\mathbf{K} \cong |0\rangle$ and when the polariton effects play an important role, as we have clarified in Subsection 7.1.2. When dealing with biexcitons we have not been speaking about polaritons at all. Is this standpoint correct? And if it is the case, then why?

Yes, this approach is basically correct for the following reason: The biexciton momentum $\hbar\mathbf{K}$ is carried away by the so-called recoil exciton, which is released during the luminescence process

$$\hbar\,\mathbf{K} = \hbar\,\mathbf{K}_{photon}(\cong 0) + \hbar\,\mathbf{K}_{exc}, \tag{8.13}$$

thereby ensuring the momentum conservation law for any value of $\mathbf{K}$. For the same reason the influence of the polariton effects (being limited to a small region $|\mathbf{K}| \leq 10^5\,\mathrm{cm}^{-1}$) on the overall emission lineshape can be, in a good approximation, neglected. From what has just been said it follows immediately that biexciton luminescence can become a very *effective channel* of radiative recombination in highly excited semiconductors, and may even take part in stimulated emission.

The typical asymmetry of the free biexciton emission lineshape in direct-gap semiconductors is documented—in addition to Fig. 8.1—also in Fig. 8.4(a) [5]. The investigated material is crystalline copper chloride, CuCl; the solid curve denotes experimental data, the dashed curve represents the theoretical lineshape (8.6) with effective temperature $T_M = 18\,\mathrm{K}$ and binding energy $E_B = 28\,\mathrm{meV}$. The presence of two lines is due to transitions to the longitudinal and transverse exciton states, split by $\Delta_{LT} \approx 5\,\mathrm{meV}$. The relevant excitation photon ($h\nu_{ex} \cong 3.7\,\mathrm{eV}$) flux was $I_{ex} = 8 \times 10^{21}\,\mathrm{photon/cm^2\,s}$ ($P_{ex} \approx 4.8\,\mathrm{kW/cm^2}$). A further increase in excitation intensity leads to biexciton collisions accompanied by a deviation of the experimental lineshape from (8.6); the line becomes more symmetric. A temperature increase entails a similar effect. For the sake of comparison, Fig. 8.4(b) displays the biexciton emission line

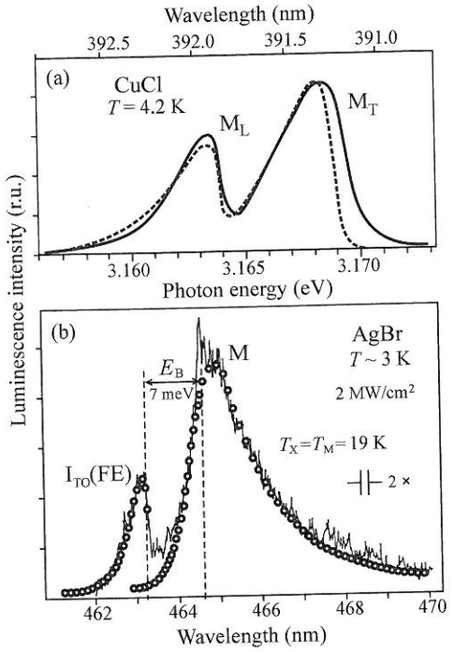

Fig. 8.4
(a) Biexciton emission spectrum in CuCl (direct-gap semiconductor) at a bath temperature of 4.2 K, excited by a pulsed N_2-laser (337 nm). Solid curve – experiment, dashed curve – theoretical lineshape after (8.6). The line $M_T(M_L)$ is due to a transition to the transversal (longitudinal) exciton level, respectively. After Grun *et al.* [5]. (b) Spectrum of edge emission of AgBr (indirect-gap semiconductor) at a bath temperature of 3 K under N_2-laser excitation, comprising a free exciton line I_{TO}(FE) and a biexciton line M. This figure demonstrates clearly the mirror symmetry of both lines. Solid curve – experiment, symbols – theoretical fit of the I_{TO}(FE) line employing (7.16) and of the M line according to (8.16), using the parameter $\Gamma = (\hbar^2/2\,a_M^2\,m_{exc})/k_B T_M$ equal to 4. The effective temperatures of the exciton and biexciton gases turn out to be equal: $T_X = T_M = 19$ K. After Baba and Masumi [6].

in an indirect-gap semiconductor (AgBr [6]); the corresponding lineshape will now be discussed.

Luminescence of excitonic molecule in an indirect semiconductor

Given the exciton band minimum located at a wavevector $\mathbf{K}_0 \neq 0$, then biexcitons are characterized by wavevectors around $2\mathbf{K}_0$. Consequently, phonons with momentum $\sim \hbar\mathbf{K}_0$ (and energy $\hbar\omega$) have to participate in the process of radiative biexciton decay. This is certainly an important difference with respect to the biexciton luminescence in direct-bandgap materials; nevertheless, we shall see that this fact has no principal impact upon the emission lineshape.

The line will be—at low temperatures—of a shape very similar to the inverse Maxwell–Boltzmann distribution. We can draw such a conclusion by looking at Fig. 8.3(b). Downward transitions from the minimum of the EM dispersion curve (where at $T \approx 0$ K the entire biexciton population occurs, having kinetic energy $\epsilon_M = 0$) give rise to photons with maximum available energy $h\nu_M = E_{gi} - E_X - E_B - h\omega$, provided the final state of the transition is located at the exciton dispersion minimum, i.e. at $\epsilon_X = 0$; all other transitions (to higher exciton states) may result in lower photon energies only. Consequently, the emission line will have a sharp high-energy threshold on the one side, and a low-energy tail on the other—as yet, everything is basically the same as in biexcitons in direct-gap semiconductors. Even so, with rising temperature now the high-energy edge will become broader, because biexcitons will gradually occupy also higher states $\epsilon_M > 0$ on their dispersion curve, and downward

transitions from these states to the minimum of the exciton states $\epsilon_X = 0$ yield photon energies higher than $h\nu_M = E_{gi} - E_X - E_B - h\omega \equiv E_0 - h\omega$.

It is obvious that also in the indirect bandgap the entire population of biexcitons is participating in the luminescence process, because the law of momentum conservation is met again, this time owing to participating phonons $h\omega$.

Let us now attempt to indicate how one can formulate a mathematical description of the emission lineshape. The concept of joint density of states cannot be—unlike the direct bandgap—introduced here. We have to deal with the task in a slightly different way, namely, in analogy with expression (5.10) that determines the luminescence lineshape of recombining free electron–hole pairs in an indirect bandgap. This expression is sufficiently universal. We can thus, making use of (5.10), write down for the case of EM luminescence in the indirect bandgap

$$I_{in}^{M}(h\nu) \cong \int \rho_M(\epsilon_M) f_M(\epsilon_M) \rho_X(\epsilon_X) f_X(\epsilon_X) \left| M_{in}^{M} \right|^2 \mathrm{d}\epsilon_M, \qquad (8.14)$$

where ϵ_M and ϵ_X stand for the biexciton and exciton kinetic energy, $\rho_M(\epsilon_M)$ and $\rho_X(\epsilon_X)$ denote the densities of states in the biexciton and exciton bands, respectively, and f_M and f_X mean the relevant occupation factors. Meanwhile, we keep the squared matrix element $|M_{in}^{M}|^2$ within the integral and we have not explicitly shown the integration limits. These can be found easily from Fig. 8.3(b). For a given constant value of $h\nu$ we have to perform the integration with respect to ϵ_M obviously from a certain lower limit to infinity; the lower limit can be derived from energy consideration (Fig. 8.3(b))

$$\epsilon_X + (h\nu + \hbar\omega) = \epsilon_M + (E_{gi} - E_X - E_B) \qquad (8.15)$$

applied for $\epsilon_X = 0$. Accordingly, making use of (8.15) yields for the lower limit

$$\epsilon'_M = (h\nu + \hbar\omega) - (E_{gi} - E_X - E_B) = h\nu + \hbar\omega - E_0.$$

We denote this lower limit as $\overline{h\nu} = h\nu + \hbar\omega - E_0$.[3] In addition, with the aid of (8.15) one can write down

$$\epsilon_X = \epsilon_M - \overline{h\nu}$$

and for the densities of states in the parabolic approximation of $\epsilon(\mathbf{K})$ we obtain $\rho_M(\epsilon_M) \approx \sqrt{\epsilon_M}$, $\rho_X(\epsilon_X) \approx \sqrt{(\epsilon_M - \overline{h\nu})}$. Thereby, expression (8.14) becomes

$$I_{in}^{M}(h\nu) \approx \int_{\overline{h\nu}}^{\infty} \sqrt{\epsilon_M}\sqrt{\epsilon_M - \overline{h\nu}}\, f_M(\epsilon_M) f_X(\epsilon_X) \left| M_{in}^{M} \right|^2 \mathrm{d}\epsilon_M.$$

In the case of bosons occupying their ground state (i.e. excitons on their dispersion curve with a local minimum at $\mathbf{K}_0$) the occupation factor f_X does not need to be taken into account. The biexciton population factor referring to the

[3] It might be of interest to note that this lower limit $\overline{h\nu}$ may be considered an analogue of the upper limit in the integral (5.10). This 'exchange' of limits arises because here the parabolas of the excited (EM) and ground (FE) states are curved in the same sense.

upper dispersion curve reads $f_M(\epsilon_M) \approx \exp(-\epsilon_M/k_B T_M)$ and the biexciton emission line is therefore described by the integral

$$I_{in}^{M}(h\nu) \approx \int_{\overline{h\nu}}^{\infty} \sqrt{\epsilon_M}\sqrt{\epsilon_M - \overline{h\nu}} \exp\left(-\frac{\epsilon_M}{k_B T_M}\right) \left| M_{in}^{M} \right|^2 d\epsilon_M. \qquad (8.16)$$

Until now we have always considered the matrix element M of the optical transition in integrals of the type (8.16) to be a constant, which can be put in front of the integral. However, this appears hardly acceptable here, for the simple reason: if $|M_{in}^{M}|^2 = \text{const}$, then (8.16) would result in a monotonic increase of the emission spectrum towards low-photon energies, which is physically impossible. Indeed, with decreasing $h\nu$ (and thus also $\overline{h\nu}$) the second term in the integrand (8.16) is increasing and, simultaneously, the integration range is getting broader while keeping all other parameters constant. Hence, various phenomenological models have been proposed to establish the dependence of M_{in}^{M} on ϵ_M or $\mathbf{K}$, i.e. $M_{in}^{M} = M_{in}^{M}(\epsilon_M) \approx M_{in}^{M}(\mathbf{K})$; this dependence should produce a rather sharp maximum of M_{in}^{M} at $\mathbf{K}_M = 2\mathbf{K}_X$. Cho [7] has proposed a matrix element of the form

$$|M_{in}^{M}|^2 = \left| \frac{C_0}{(\mathbf{K}_M/2 - \mathbf{K}_X)^2 + (1/a_M)^2} \right|^2, \qquad (8.17)$$

where $C_0 = \text{const}$ and a_M stands for 'biexciton radius', or the average separation of the two holes in a biexciton. In other words, a_M is a quantity determining the spatial extent of the biexciton wavefunction; as such, it is of the same order of magnitude as the exciton Bohr radius a_X. The underlying physical background of expression (8.17) consists in the fact that the matrix element drops rapidly from its maximum value at $\mathbf{K}_M = 2\mathbf{K}_X$ down to almost zero just for $|\mathbf{K}_M/2 - \mathbf{K}_X| \approx a_M^{-1}$. This reflects the 'magnitude' of the biexciton in real space. The radius a_M thus becomes a crucial factor driving the emission lineshape; this factor is usually embodied in the dimensionless parameter $\Gamma = (\hbar^2/2\, a_M^2\, m_{exc})/k_B\, T_M$. A detailed discussion of the emission lineshape (8.16) employing the matrix element (8.17) together with a hint for numerical integration can be found in Appendix C.

Figure 8.4(b) shows the emission spectrum of AgBr in the edge emission region, acquired under high photoexcitation with a pulsed nitrogen laser. The spectrum contains two lines—an I_{TO}(FE) line, ascribed to radiative decay of a free exciton accompanied with the emission of a TO-phonon, and an M-line being due to radiative decay of a biexciton. It is commonly supposed that biexciton annihilation is, apart from photon emission, accompanied with the emission of the same type of phonon as free exciton decay, i.e. a TO-phonon in this case. The biexciton line here therefore would have been correctly denoted as I_{TO}(M) or I_{TO}(EM) rather than simply M, if one insisted on strictly adhering to notation.[4] Theoretical fits (symbols) follow the experimental

[4] It can be shown that a biexciton has in most cases the same full symmetry as the crystal ground state (Γ_1), hence the selection rules for biexciton and exciton luminescence are similiar to each other.

data more than satisfactorily. It is seen that the typical M-line asymmetry—broadening towards the long-wavelength side, i.e. a resemblance to the inverse Maxwell–Boltzmann distribution—is indeed conserved even in indirect-gap semiconductors.

M-line intensity dependence

Apart from the lineshape analysis, the behaviour of the M-line as a function of the photoexcitation power density represents an important auxiliary guideline for firm identification of the experimentally observed biexciton emission line. Intuitively we should expect this dependence to be quadratic. Although experiment does confirm the dependence of the biexciton luminescence intensity upon the excitation intensity to be superlinear, $I^M \sim I_{ex}^{n}$, the exponent n amounts to only $n \cong 1.4$–1.6 in most cases. This rule holds independently of whether the forbidden gap is direct or indirect; $n = 2$ is seldom attained. An explanation has been put forward by the Knox *et al.* [8] through a kinetic theory, similar to the model discussed in Section 3.5, which describes the simultaneous occurrence of both monomolecular (here exciton) and bimolecular (here biexciton) luminescence. The authors [8] divide excitons photogenerated by band → band transitions into 'optical' and 'thermal' ones, supposing that biexcitons can be created by fusing thermal excitons only. They arrive at the M-line intensity dependence

$$I^M \approx \text{const}(\sqrt{1 + I_{ex}/I_0} - 1)^2, \qquad (8.18)$$

where I_0 stands for the characteristic material-dependent excitation intensity. Evidently, for $I_{ex} \ll I_0$ we can approximate $\sqrt{1 + I_{ex}/I_0} \approx 1 + I_{ex}/2\, I_0$ and I^M scales with I_{ex} quadratically, while for $I_{ex} \gg I_0$ the dependence (8.18) turns out to be linear: $I^M \sim I_{ex}$. This corroborates qualitatively the experimental observations; the reader is reminded about the resemblance of (8.18) to relations (3.24) and (3.26). Simultaneously the model [8] predicts that the intensity dependence of free exciton luminescence should be linear, also in accordance with experiment.

Figure 8.5 shows the superlinear growth of biexciton luminescence in AgBr ($I^M \sim I_{ex}^{1.5}$). It may be of interest to specify the relevant experimental conditions [9]. The excitation was performed by ~ 2 ns pulses of a dye laser, the I_{TO}(FE) and M lines were observable only in a temporal window coincident with the laser pulse; then the emission spectra and the intensity dependence were recorded. Further development of the spectra with increasing delay after the excitation pulse, recorded with the use of time-resolved spectroscopy, is displayed in Fig. 2.48. It can be seen how the fast edge emission I_{TO}(FE) and M fades away, free excitons and biexcitons become gradually localized on the iodine ions and a slower emission band emerges at 500 nm, due to excitons localized on the isoelectronic impurity I^-.

To confirm further the interpretation of the emission M-line as being due to EM decay, it is highly recommended to analyse its spectral position and temperature behaviour. They are closely connected with the determination of two important EM parameters: the binding energy E_B and the radius a_M.

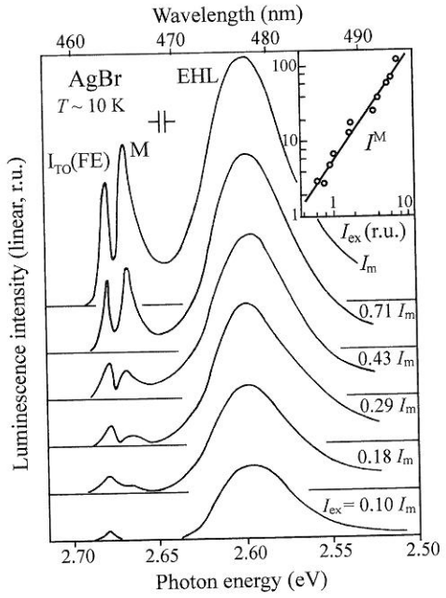

Fig. 8.5
Edge emission of AgBr under pulsed laser excitation at a bath temperature of $T \approx 10\,\mathrm{K}$. The nonlinear growth of the biexciton M-line with increasing excitation intensity I_{ex} (I_m corresponds to $\approx 0.7\mathrm{MW/cm^2}$) is clearly observable. The inset demonstrates the dependence of the integral M-line intensity $I^M \sim I_{ex}^{1.5}$. The I_{TO}(FE) line is due to free exciton decay, and the EHL line originates in the electron–hole liquid. After Pelant *et al.* [9].

8.2.2 Determination of biexciton parameters

The biexciton binding energy E_B in direct-bandgap semiconductors can be extracted readily and quite accurately from the emission spectrum. According to (8.5), E_B is equal to the energy separation between the emission line of a free exciton–polariton and that of a biexciton, or more precisely, to the separation between the centre of the polariton line and the high-energy edge of the biexciton line.

Less obvious is how to determine E_B in a semiconductor with an indirect bandgap. There, the high-energy edge of the M-line gets broader at $T > 0\,\mathrm{K}$, as discussed in the context of Fig. 8.3(b). Fortunately the model [7], making use of the matrix element (8.17), comprises in the theoretical curve not only the relevant lineshape but also an energy position pertinent to the minimum of the biexciton dispersion $\epsilon_M(\mathbf{K})$. This position is indicated in Fig. 8.4(b) by a vertical line at 2.669 eV ($\sim 464.5\,\mathrm{nm}$). The determination of E_B is then the same as mentioned above: as the energy separation of this line from the energy coordinate pertinent to the minimum of the exciton dispersion $\epsilon_X(\mathbf{K})$, i.e. from the vertical line at 2.676 eV ($\sim 463.2\,\mathrm{nm}$). This is how we get $E_B \approx 7\,\mathrm{meV}$ in AgBr.

This mode of assessing the EM binding energy is designated as *spectroscopic*. An independent determination of E_B consists in investigating the intensity variations of the FE and M lines with varying temperature and can thus be called a *thermodynamic* method. It is applicable above all in indirect bandgap semiconductors where the free exciton emission line is sufficiently strong. The principle is as follows: In the course of sample heating, biexcitons undergo thermal dissociation more easily than free excitons do, because their binding energy is always smaller, $E_B < E_X$. Due to this, the M-line intensity

drops substantially faster compared with the intensity fall of the FE-line. In thermodynamic equilibrium, and provided a quadratic proportion $I^M \sim I_{ex}^2 \sim (I^{FE})^2$ is valid, we can anticipate that the intensity ratio $R = (I^{FE})^2/I^M$ will be apparently driven by a factor $\exp(-E_B/k_B T_M)$. A more exact derivation leads to the even sharper dependence

$$R = \frac{(I^{FE})^2}{I^M} \approx T_M^k \exp\left(-\frac{E_B}{k_B\, T_M}\right), \tag{8.19}$$

where the value of the exponent k varies depending on whether the free movement of the quasi-particles FE, EM is not limited in any way ($k = 3/2$) or whether they are localized in a certain place of the sample, for instance in a potential well created by a local deformation of the sample ($k = 3$) [10]. A semi-logarithmic plot of $R^* = (I^{FE})^2/I^M T_M^k$ against $1/k_B T_M$ then yields E_B as the slope of the straight line.

Such a plot is shown in Fig. 8.6 for crystalline silicon at three different levels of laser excitation [10]. It can be seen that the slope, i.e. the binding energy E_B, is independent of the excitation intensity (in fact, there is no reason why it should be dependent); we get $E_B = 1.53\,\mathrm{meV}$, in good agreement with spectroscopic value $E_B = 1.46\,\mathrm{meV}$. In this case the exponent $k = 3$ was applied in (8.19), because the gas of free excitons and biexcitons was spatially localized in a potential well. This localization made it possible to attain sufficiently elevated concentrations of both FE and EM under not excessive optical pumping levels. As a consequence of this approach a purely quadratic dependence $I^M \sim I_{ex}^2 \sim (I^{FE})^2$ was observed in experiment—since the condition $I_{ex} \ll I_0$ was fulfilled in (8.18)—justifying the use of eqn (8.19).

It is worth mentioning that experimentally observed binding energies E_B in various materials systematically exceed theoretical values. This is documented in Table 8.1 (the only exception to this rule being copper halides CuCl and CuBr). The reasons are not clear. Often one blames the theoretical approaches for not taking into account at least two factors: (i) the effect of lattice polarization in polar semiconductors, which may raise E_B substantially and (ii) the process of creating a biexciton from two excitons located at different valleys of the conduction (valence) band in indirect semiconductors. For in this way one can generate a two-electron triplet spin function connected with a lower

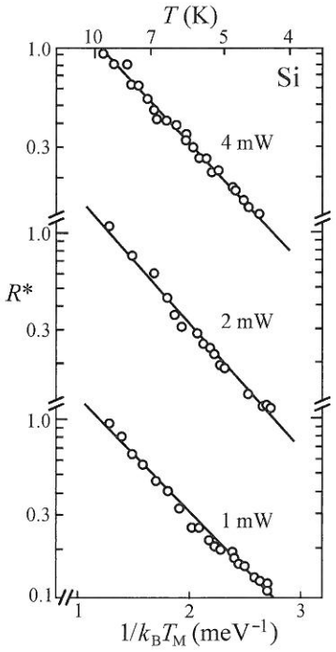

Fig. 8.6
Thermodynamic determination of the EM binding energy in silicon at three levels of laser excitation. Symbols—experiment, lines—fit by the quantity $R^* = R/T_M^3$ with the use of (8.19). Taking into consideration the relatively long lifetimes of participating quasi-particles along with not too high excitation, $T_M = T$ (bath temperature) holds. After Gourley and Wolfe [10].

Table 8.1 Comparison of the experimental and theoretical values of EM binding energy in several semiconductors (d – direct bandgap, i – indirect bandgap). The values of E_B are given in meV.

Semicondutor	E_B experimental	E_B calculated
CuCl (d)	28–34	41–44
AgBr (i)	~ 7	1.3–2.5
CdS (d)	~ 5	2–5
ZnO (d)	12–16	5–9
GaAs (d)	~ 0.7	~ 0.4
Si (i)	1.2–1.5	0.45–1.1
Ge (i)	~ 0.3	~ 0.1
HgI_2 (d)	~ 6	~ 2.5

lying energy level compared with a singlet state of two excitons located in the same valley (there, conforming to the Pauli exclusion principle, two electrons must be of antiparallel spins, i.e. total spin $S = 0$). Thereby the EM dispersion curve in Fig. 8.3(b) may shift downwards, raising the binding energy E_B.

The above considerations are in qualitative agreement with Table 8.1. The most marked difference between the experimental and theoretical values of E_B occurs in AgBr, where—as in a polar, indirect-gap semiconductor—both factors enter the play. Any quantitative theoretical estimates are lacking, though.

The second biexciton parameter, the radius a_M, can be found relatively easily from luminescence measurements in indirect semiconductors. When fitting the experimental lineshape with relations (8.16) and (8.17), the variable parameters are $\Gamma = (\hbar^2/2a_M^2\, m_{exc})/k_B\, T_M$ together with the reduced wavelength axis $\overline{h\nu}/k_B T_M = (h\nu + \hbar\omega - E_0)/k_B\, T_M$ [7]. This enables an independent determination of both T_M and a_M. The fit shown in Fig. 8.4(b) yields, for AgBr, $\Gamma = 4$, $T_M = 19\,K$ and $a_M \approx 2.6\,nm$. In direct-bandgap semiconductors, on the other hand, there is no similar straightforward and commonly accepted method to establish a_M experimentally.

The last remark in this section concerns *bound* (*localized*) biexcitons. It has been found that free biexcitons, similarly to free excitons, can get localized close to impurity atoms. Actually, this is not surprising if we recall bound multiexciton complexes (Subsection 7.2.1). A bound biexciton can be regarded as a limiting case of a bound exciton complex composed of two excitons, even though the process of creation (localization) may be slightly different. In the case of high excitation, biexcitons as a whole get localized preferentially. The relevant emission line, originating in radiative decay of bound biexcitons, is red-shifted with regard to $(E_{g(i)}–E_X–E_B)$ and features properties analogous to other extrinsic radiative channels, namely, its shape is symmetric, does not vary either with excitation intensity or temperature and the line exhibits saturation behaviour.

Bound biexcitons have been discovered via luminescence measurements in GaP, CuCl and AgBr.

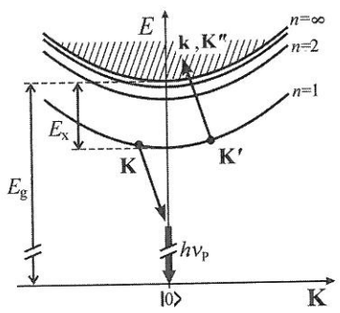

Fig. 8.7
Free exciton collisions in the $E(\mathbf{K})$ scheme. $\mathbf{K}$, $\mathbf{K}'$ denote the exciton wavevectors before the collision, $\mathbf{k}$ is pertinent to internal e–h pair movement ($h^2k^2/2m_r$) and $\mathbf{K}''$ to its translation movement ($h^2K''^2/2(m_e + m_h)$) after the collision.

8.3 Collisions of free excitons

Another type of interexciton interaction that can manifest itself in luminescence spectra at higher excitation power densities is inelastic collisions between free excitons (X–X collisions). Two FEs, instead of fusing and creating an EM, collide with one another while one of the two FEs dissociates into a free e–h pair and the remaining one recombines radiatively emitting a photon $h\nu_P$. This photon energy, however, is reduced compared to the $n = 1$ FE state by an amount passed over to the first exciton and making it dissociate—and this is the very exciton binding energy E_X.

Let us consider a direct-bandgap semiconductor, Fig. 8.7. Energy balance then reads

$$2 \text{ free excitons} \rightarrow \text{photon} + \text{free } e\text{–}h \text{ pair}$$

$$(E_g - E_X) + (E_g - E_X) \approx h\nu_P + (E_g + E_{e,h}^{kin}),$$

and thus

$$h\nu_P \approx (E_g - 2\,E_X) - E_{e,h}^{kin}, \tag{8.20}$$

where $E_{e,h}^{kin} = \hbar^2 k^2/2\,m_r + \hbar^2 K''^2/2\,(m_e + m_h)$ stands for the kinetic energy of the created electron–hole pair. A new emission P-line therefore appears, red-shifted from the spectral position of an exciton–polariton (which is E_g–E_X) roughly by E_X(see Fig. 8.1 and Problem 8/1).

Experiment reveals that the final state in this collision process does not necessarily have to be always a free e–h pair. The exciton, acquiring energy at the collision, may happen to be excited only to some higher lying but still bounded exciton state ($n = 2, 3, 4, \ldots$) and the energy of the emitted photon is then

$$h\nu_{Pn} \approx (E_g - E_X) - E_X(1 - 1/n^2),\ n = 2, 3, \ldots, \infty, \tag{8.21}$$

which is nothing but a generalization of (8.20) with simultaneous neglect of kinetic energy. In Fig. 8.8 there are emission spectra of a high-purity monocrystalline ZnO sheet under high excitation with an electron beam at $T = 10\,K$ [11]. Owing to the extreme purity, the emission line of the exciton localized on a residual impurity (denoted I_9) is strongly suppressed, enabling the observation of two lines in the P-band, corresponding to photon energies $h\nu_{P2}$ and $h\nu_{P\infty}$ according to (8.21).

The basic features of the spectral shape of the emission line accompanying the creation of a free e–h pair ($n = \infty$) can be readily guessed: The P_∞ line should have a high-energy threshold at E_g–$2E_X$ and is expected to be asymmetrically broadened towards the low-energy side, since for the e–h pairs there exists a continuum of energy states. The creation of an e–h pair with high kinetic energy $E_{e,h}^{kin}$ then leads, in compliance with (8.20), to the emission of lower-energy photons.

Moriya and Kushida studied this lineshape theoretically in the framework of perturbation theory and found that [12]

$$I_{sp}^{P\infty}(h\nu) \approx \left| M^P \right|^2 h\,\nu^3\, n_X^2 \int_0^\infty d\xi \int_0^\infty dt\, \frac{\xi^{1/2}}{(1 + \xi/E_X)^4}$$

$$\times \exp\left[-t - \frac{1}{4t}\left(\frac{E_g - 2\,E_X - h\nu - \xi}{k_B\,T}\right)^2\right] \tag{8.22}$$

(M^P denotes the optical matrix element and n_X the concentration of free excitons). The physical meaning of the double integration in (8.22) consists in the fact that photons with a given energy $h\nu$ may originate from numerous combinations of initial ($\mathbf{K}$, $\mathbf{K}'$) and final ($\mathbf{k}$, $\mathbf{K}''$) wavevector pairs. In practise, however, this theoretical lineshape is seldom compared with experiment. There are several reasons for this. On the one hand, a background composed of many lines due to impurities (BE, e–A^0, h–D^0, etc.) often occurs in this spectral region, which makes the lineshape analysis of the P-line difficult; on the other hand, the very theoretical expression (8.22) is based on a simplified approximation of the interaction potential between the two excitons which is,

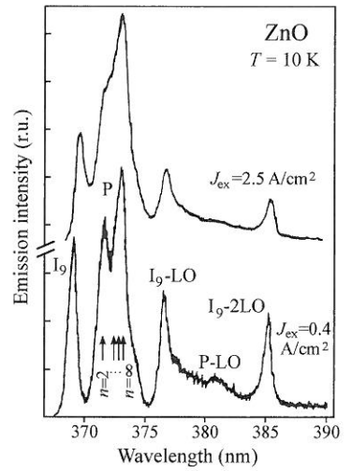

Fig. 8.8
Emission spectra of pure ZnO under electron beam excitation (40 kV, ~ 100 ns pulses) with two different current densities J_{ex}. Apart from the P-band, the bound exciton line I_9 and its LO-phonon replicas can be seen. The P-band grows superlinearly with increasing excitation current density at the expense of other lines. Arrows indicate emission wavelengths calculated using (8.21) for $n = 2$, 3, 4, and ∞. $T = 10\,K$. After Hvam [11].

in reality, rather complicated. It is worth noting that (8.22) contains a term n_X^2, therefore one can expect a quadratic dependence of I_{sp}^P upon the excitation intensity; Fig. 8.8 basically confirms this expectation.

The close resemblance of the M- and P-lines (superlinear growth, line asymmetry) invokes the following questions: When can we in an experiment expect the creation of excitonic molecules and when are inelastic exciton collisions more likely to occur? Or do both of these mechanisms take place always simultaneously, as Fig. 8.1 indicates?

The answer to these questions is neither simple nor unambiguous. There is no strict theoretical prediction as to when (at what excitation level) and where (in what material) we should expect this mechanism or that one to occur. Of course, in a qualitative manner we can come to the conclusion that the fusion of two excitons into an EM will prevail at relatively lower excitation power densities and provided E_B is sufficiently large. For if we create a very high concentration of free excitons possessing, moreover, a non-equilibrium excess kinetic energy ('optical excitons' introduced in Subsection 8.2.1), then the collision process will probably predominate. (The interacting excitons will 'have no time' to fuse; only a collision followed by one exciton annihilation will set in.) The observed predominance of exciton collisions under pumping with high current density electron beams seems to support this conjecture. However, there is certainly a relatively broad range of laser excitation power densities where both 'M' and 'P' actions occur simultaneously. Radiative decay of the EM as well as luminescence due to exciton collisions can easily result in stimulated emission, as we shall see later.

All considerations held in this section concerned direct-badgap semiconductors. Till now the P-line has not been observed in any indirect-bandgap material (Problem 8/3). On the contrary, in the next section we shall discuss a luminescence process taking place exclusively in indirect semiconductors, namely, radiative annihilation of an electron–hole liquid.

8.4 Electron–hole liquid (EHL)

Another qualitative alteration of luminescence (but not only luminescence) behaviour of a semiconductor, linked with high exciton densities, is exciton condensation into a new state of matter, named an *electron–hole liquid*, EHL. We have already introduced the concept of an exciton gas; the condensation of excitons represents a phase transition that can be regarded as a quantum-mechanical analogue of the well-known classical gas condensation into a liquid (water vapour molecules in the atmosphere condense into droplets constituting fog or rain). In the case of excitons one speaks of a Fermi liquid—a degenerate electron–hole system—composed of free fermions, electrons and holes. Similarly to the classical case, also particles of this particular liquid form spherical drops, inside which they are held together by means of internal forces and surface tension; hence also the term *electron–hole drops* (EHD) is sometimes used.

The typical diameter of these drops amounts to several μm. It should be stressed again that the drops do not contain excitons but free electrons and

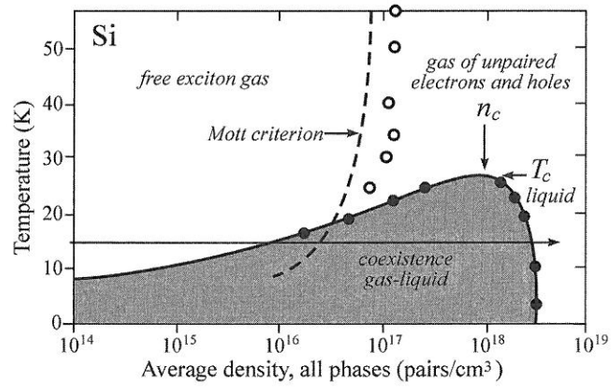

Fig. 8.9
The phase diagram of photoexcited electrons and holes in silicon. It can be deduced, e.g., that for an average *e–h* pair density of $\sim 10^{17}$ cm^{-3} and $T = 15$ K a saturated free exciton gas with a density about 10^{16} cm^{-3} coexists with drops of EHL; in each of these drops there is a concentration of *e–h* pairs $\sim 3 \times 10^{18}$ cm^{-3}. The dashed curve and open symbols denote theoretical and experimental values of the Mott insulator–metal transition (Section 8.5). After Shah *et al.* [13].

holes. The thing is that excitons in the condensate immediately 'break up', therefore the designation 'exciton drops', which is sometimes used, is not correct. The density of *e–h* pairs inside the drops may be higher by several orders of magnitude than the concentration of excitons remaining in the surrounding gas phase, as we shall see shortly.

To liquefy a classical gas, it is necessary to reach a critical pressure and to descend below a critical temperature, the whole process being advantageously sketched in a p, T (pressure, temperature) diagram. As for the exciton concentration, it appears more illustrative to apply an n, T (density, temperature) coordinate system and to speak about the critical density n_c of *e–h* pairs and the critical temperature T_c of the liquid. The phase diagram of an electron–hole system in silicon is shown in Fig. 8.9. The values of the critical temperature and the critical density are $T_c = 25$ K and $n_c = 1.2 \times 10^{18}$ cm^{-3}, respectively. An EHL cannot survive for $T > T_c$.

The *e–h* pair density in EHL at a given temperature is driven by the liquid interface of the two-phase coexistence region (shadowed area), where the *e–h* system separates into a liquid and the surrounding gas phase. It can be seen that this density is $n_0 \approx 3 \times 10^{18}$ cm^{-3} and is only weakly temperature dependent in the range 0–15 K. On the left and above the coexistence region only the gas of free excitons may subsist.

Similarly to the case of excitonic molecules, of fundamental importance is now to ask about the stability of the EHL, or to ask which parameter plays the role of the binding energy E_B here. Prior to establishing such a parameter, we define the ground state energy $E_G(n)$ of the liquid, allotted per one *e–h* pair. This energy is given by the sum of the kinetic, exchange and correlation energies and it exhibits, as a function of the *e–h* pair density, its minimal value at the equilibrium density n_0. Should the EHL be a stable and energetically favourable phase compared to the free exciton gas, this minimum must be located deeper than the ground exciton state level, referred to the bottom of the *e–h* continuum of states. In Fig. 8.10, this means that the relation $|E_G(n_0)| > E_X$ must hold. The difference $\varphi = |E_G(n_0)| - E_X$ then represents the (material dependent) EHL stability parameter we are looking for. φ is called the binding energy of the condensate with respect to free excitons (or, in analogy with thermionic electron emission, the *work function*). It is the energy

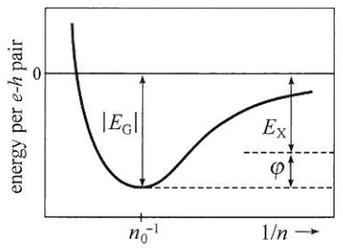

Fig. 8.10
Schematic drawing of the EHL ground state energy per electron–hole pair as a function of the reciprocal pair density.

required to 'evaporate' one e–h pair from the liquid.[5] The condensate is stable if and only if $\varphi > 0$.

Various theoretical approaches to calculate $E_G(n)$ or φ, along with obtained results, are summarized, e.g., in [14] and [15]. Theory reveals that the EHL stability may profit from specific features of the energy band structure of indirect-bandgap semiconductors. In particular, the long exciton lifetime and several equivalent conduction band minima ν_c, in, e.g., Si and Ge (or several equivalent valence band maxima ν_v in AgBr) promote the chance of photoelectrons (photoholes) to reduce efficiently their kinetic energy. This entails an important increase in stability and cohesiveness of the condensed phase. Quantitatively, the increased number of equivalent band extremes ν_c (ν_v) appears in the expression for the density of states in the bands. Instead of (5.4) we have to be more specific now and write down

$$\rho_c(E) = \nu_c \frac{(2\,m_{de})^{3/2}}{2\pi^2\hbar^3}\, E_e^{1/2},$$

$$\rho_v(E) = \nu_v \frac{(2\,m_{dh})^{3/2}}{2\pi^2\hbar^3}\, E_h^{1/2}. \qquad (8.23)$$

The factors ν_c and ν_v describe the fact that the electrons and holes have at their disposal ν_c-times or ν_v-times more available states, respectively, in comparison with a semiconductor having a single band extreme. (In a semiconductor characterized by a simple band structure with a direct bandgap at the Γ point, $\nu_c = \nu_v = 1$ holds, while in silicon $\nu_c = 6$, $\nu_v = 2$.) Furthermore, instead of simple effective masses m_e, m_h, which belong to idealized parabolic bands, we have to consider now the so-called density-of-states effective masses m_{de}, m_{dh} that take into account the complex band structure of real semiconductors Si, Ge, AgBr, etc. Namely, they involve the anisotropy of the effective mass and the existence of heavy and light holes with markedly different masses [14].

The kinetic energy of photocarriers gets reduced because its mean value is equal to $3/5F_e$ and $3/5F_h$(F_e, F_h being the Fermi energies of electrons and holes, respectively), see Problem 8/4. A pure mechanical analogue may be invoked: if we pour a liquid (here the photoexcited electron–hole fluid) uniformly into several vessels (here several valleys of the conduction or the valence band) instead of a single one, the liquid levels in the vessels become inversely proportional to the number of vessels used.

It has been demonstrated that further promotion of φ arises from the interaction of electrons and holes with LO-phonons. A very stable EHL with a high T_c therefore occurs in polar semiconductors with an indirect bandgap (AgBr, GaP). On the contrary, the short exciton lifetime along with the single conduction band valley in the Γ point of direct semiconductors do not allow the necessary conditions for exciton condensation to be reached, even though this issue had been intensively discussed throughout the 1970s and 1980s.

[5] Upon leaving the condensate, such a pair is immediately bound and creates a free exciton.

8.4.1 Luminescence determination of EHL parameters

The EHL represents an electronic excited state of a semiconductor, which fades away rapidly (10^{-9}–10^{-6} s) after the cessation of the excitation effect. However, the EHL emits its characteristic luminescence radiation that originates (even in the steady state) through the radiative recombination of electrons and holes constituting the condensate. The probability of radiative recombination in the EHL is even increased several times compared to a system of free carriers of the same density (due to the so-called enhancement factor) because of the correlation existing between the electrons and holes. The EHL luminescence is of intrinsic type and its emission spectrum features a relatively broad band rather than a single narrow line; this reflects the Pauli exclusion principle, according to which each level in a system of fermions can be occupied by two electrons (or holes) at the most (Fig. 8.11). Referring to what has been discussed above, this band appears in the emission spectrum as soon as the pumping level exceeds a certain threshold level, provided the condition $T < T_c$ holds at the same time.

Let us now discuss what the emission bandshape looks like; simultaneously we shall learn how we can, by analysing the emission spectrum, extract the two most important EHL parameters, namely, n_0 and φ. These are listed, for selected semiconductors, in Table 8.2.

The formation of EHL luminescence is evident from Fig. 8.11. The emission lineshape is defined through a combination of all the occupied electron states with all the occupied hole states, the momentum conservation rule for all recombining e–h pairs being ensured through the participation of a phonon $\hbar\omega$. Formally therefore we can start with the convolution integral (5.10) that has been derived for allowed indirect recombination processes

$$I^{EHL}(h\nu) \approx |M|^2 \int_0^{\overline{h\nu}} \sqrt{E}\sqrt{\overline{h\nu} - E}\, f_c(E)\; f_v(\overline{h\nu} - E)\mathrm{d}E, \qquad (8.24)$$

and where $\overline{h\nu} = h\nu + \hbar\omega - E_g$.

Now we perform in (8.24), compared to (5.10), two formal adjustments and then one essential physical modification.

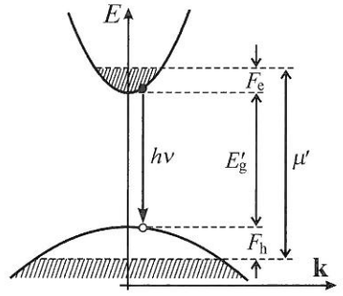

Fig. 8.11
Schematic of EHL recombination radiation. A photon $h\nu$ originates via the recombination of an electron with a hole from the corresponding Fermi seas. Electrons occupy the conduction band up to the electron Fermi level F_e; in a similar manner levels in the valence band are occupied by holes up to the hole Fermi level F_h. E'_g means a reduced bandgap ($< E_g$). For the sake of simplicity the transitions are drawn as direct transitons. $\mu' = E'_g + F_e + F_h$ stands for the EHL chemical potential.

Table 8.2 The basic EHL parameters of selected semiconductors (experimental values); n_0, φ and T_c denote the equilibrium density, the binding energy and the critical temperature, respectively.

Semiconductor	n_0 (cm^{-3})	φ (meV)	T_c (K)
Ge	2.4×10^{17}	1.5	6.5
Si	3.3×10^{18}	8	25
GaP	6×10^{18}	15	40
AgBr	8×10^{18}	55	~ 60 ($T_{ef} \approx 100$)(1)
TlBr(2)	1.4×10^{19}	–2.2	–

Note: (1) Owing to the short lifetime, the effective critical temperature T_{ef} is higher than the bath T_c.
(2) Theoretically calculated values.

Under formal adjustments we omit the phonon energy $\hbar\omega$ in (8.24) and replace E_g by the so-called reduced or renormalized bandgap $E'_g < E_g$; therefore we put $\overline{h\nu} = h\nu - E'_g$. The omission of $\hbar\omega$ serves only to simplify our reasoning; this step does not affect the emission spectral shape, shifting it only—as a whole—on the photon energy axis. Graphically, we can then illustrate the EHL recombination radiation as if it were due to direct transitions (Fig. 8.11); we shall see later that this simplification will turn into a certain benefit. Introducing the reduced bandgap E'_g has a deeper physical meaning: it tells us that the high density of e–h pairs inside the condensate droplets entails a reduction of the bandgap E_g (calculated within the one-electron approximation or found experimentally, e.g. with the aid of optical measurements using low-intensity light) down to a value $E'_g < E_g$. We shall investigate this effect more closely in Section 8.5. For luminescence measurements, this has a practical consequence, namely, the recombination radiation originating inside the drops is not absorbed in the surrounding lattice and can be easily detected.

The essential physical modification, indicated above, compared to the luminescence of an e–h system under weak excitation (Subsection 5.2.2) consists now in introducing into (8.24) for f_c and f_v the relevant Fermi–Dirac distribution functions in the conduction and the valence bands, respectively. Therefore, (8.24) becomes

$$I^{\mathrm{EHL}}(h\nu) \approx \int_0^{\overline{h\nu}} \sqrt{E}\sqrt{\overline{h\nu} - E}\left[\exp\left(\frac{E - F_e}{k_B T}\right) + 1\right]^{-1} \left[\exp\left(\frac{\overline{h\nu} - E - F_h}{k_B T}\right) + 1\right]^{-1} \mathrm{d}E. \qquad (8.25)$$

The integrand does not contain any singularities and thus to calculate (8.25) for fitting the experimental emission spectrum, any simple numerical method may be used.

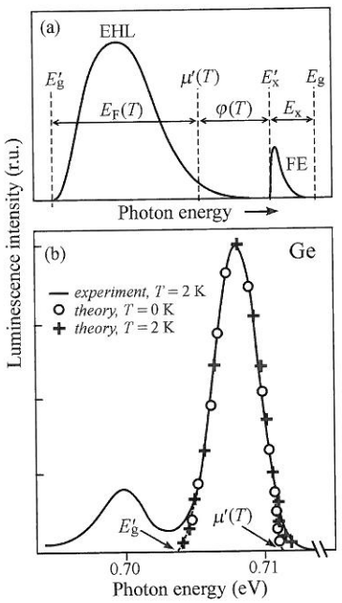

Fig. 8.12
(a) Schematic of the emission spectrum comprising the EHL band and a free exciton line FE, indicating at the same time how to determine the binding energy φ. (b) Experimental and theoretical (eqn 8.25) lineshapes of the EHL band (LA-phonon replica) in pure Ge. The FE line is not displayed. The less-intense band at ~ 0.7 eV is a TO-phonon replica of the EHL luminescence. After Benoit à la Guillaume and Voos [16].

Determination of the reduced bandgap E'_g and the potential μ'

Close to the temperature $T = 0$ K, the emission spectrum obviously starts on the short wavelength side at $h\nu = \mu'$ and terminates on the long-wavelength side at $h\nu = E'_g$ (let the reader compare Figs 8.11 and 8.12(a)). Photoluminescence therefore turns out to be a unique method for a direct determination of auxiliary EHL parameters such as the reduced bandgap E'_g and the chemical potential of the electron–hole liquid $\mu' = E'_g + F_e + F_h$.

The fit parameters[6] in (8.25) are F_e, F_h and T. They are not independent of each other, however, which somewhat complicates the fitting procedure based on eqn (8.25). This procedure is connected with the extraction of the density n_0 from the luminescence spectrum, a process that we are now going to describe.

[6] E'_g appears to be also a fit parameter, however, it does not affect the bandshape but shifts the overall spectrum on the wavelength axis only. It can be extracted from the final fitting of the calculated curve on the experimental spectrum.

Determination of the electron–hole density n_0

The simplest way to determine n_0 can be realized at very low temperatures. Let us consider the limit case $T = 0$ K. The EHL emission band has a full width (at its foot) $E_F = F_e + F_h = \mu' - E'_g$ (Figs 8.11 and 8.12). From here, n_0 will be extracted as follows: The electron density n_e (= the hole density n_h) is given by summing over all occupied states in unit volume, which is generally expressed as

$$n_0 = n_e = n_h = \int_0^\infty \rho_c(E) f_c(E, F_e)\,\mathrm{d}E = \int_0^\infty \rho_v(E) f_v(E, F_h)\,\mathrm{d}E$$

and, by considering explicitly the densities of states (8.23), the above expression transforms into

$$n_0 = n_e = n_h = \frac{\nu_{c(v)}(2m_{de(h)})^{3/2}}{2\pi^2\hbar^3} \int_0^\infty \sqrt{E}\left[\exp\left(\frac{E - F_{e(h)}}{k_B T}\right) + 1\right]^{-1} \mathrm{d}E. \qquad (8.26)$$

For $T = 0$ K (and solely in this case) the integration can be performed analytically which yields

$$n_0 = \frac{\nu_c}{3\pi^2\hbar^3}(2m_{de}F_e)^{3/2} = \frac{\nu_v}{3\pi^2\hbar^3}(2m_{dh}F_h)^{3/2} \qquad (8.27a)$$

or

$$\nu_c^{2/3} m_{de} F_e = \nu_v^{2/3} m_{dh} F_h. \qquad (8.27b)$$

Ultimately the relationship between the full width of the band E_F and the concentration n_0 follows from $E_F = F_e + F_h$, which combined with (8.27b) gives

$$F_e = \left[1 + \left(\frac{\nu_c}{\nu_v}\right)^{2/3} \frac{m_{de}}{m_{dh}}\right]^{-1} E_F. \qquad (8.28)$$

Therefore, upon obtaining experimentally the full width E_F of the emission band we are able, making use of (8.27a), (8.28) and of the band structure parameters, to calculate n_0 immediately. It can be seen that $n_0 \sim E_F^{3/2}$; the wider the luminescence band, the denser the EHL.

For $T \neq 0$ K the procedure is similar, the expression (8.26) being no longer computable analytically, though. The integration has to be performed numerically. The method of determining n_0 then cannot be separated from fitting the emission bandshape, as we have already mentioned.

The experimental EHL band is fitted with the aid of (8.25), letting the values of the couple F_e, F_h vary, but keeping their ratio fixed, as follows from the numerical integration of (8.26) or, in other words, from the condition of the electroneutrality of the condensate $n_e = n_h$. (This means that the e–h pair density $n_0 = n_e = n_h$ enters the spectral shape (8.25) implicitly.) The temperature T represents the next fit parameter, as already mentioned above; this effective temperature can again be higher than the lattice temperature. It should be noted, however, that at a sufficiently low bath temperature the simple

determination of n_0 through a combination of (8.27) with an iterative analytical calculation of the bandshape (8.25) for $T = 0\,\mathrm{K}$ is often applicable. That is to say, the spectral shape undergoes only an insignificant modification around μ', as demonstrated in Fig. 8.12(b) [16].

Determination of the binding energy φ

From the above fitting procedure one gets the value of the reduced bandgap E'_g together with $F_e(T)$ and $F_h(T)$. Their sum defines the chemical potential: $\mu'(T) = E'_g + F_e(T) + F_h(T)$. We shall show before long that μ' is the *spectroscopic energy* characterizing the EHL ground state, i.e. it corresponds to the energy $E_G(n_0)$. Then it is readily seen in Figs 8.10 and 8.12(a) that the condensate binding energy φ (with respect to a free exciton) may be extracted very simply as the separation between μ' and the low-energy edge of the FE emission line, whose spectroscopic position is denoted E'_X in Fig. 8.12(a):

$$\varphi(T) = E'_X - \mu'(T).^7 \tag{8.29}$$

Why, then, does $\mu'(T)$ characterize the EHL ground state? We come to this conclusion by means of simplified reasoning, the origin of which is ascribed to Keldysh: the maximum EHL luminescence photon energy at $T = 0\,\mathrm{K}$ is determined by the radiative recombination of an electron with a hole which reside on their Fermi levels; in other words, such recombination leaves the EHL in its ground state (any other recombination event leaves behind the EHL in an excited state, because for instance an unoccupied state at energy lower than F_e appears in the electron Fermi sea, and a redistribution of the population on electron levels must follow to restore the ground state). Consequently, μ' is the spectroscopic energy relevant to the EHL ground state. This can also be shown computationally (Problem 8/5).

This determination of φ is essentially spectroscopic, much like the case of the determination of the binding energy E_B of an excitonic molecule. Similarly, also here the possibility exists to set φ thermodynamically. In this case φ is obtained as the activation energy from plotting, e.g., the exciton density on the gas–liquid boundary against temperature (Fig. 8.9). The excellent treatise of these methods as well as of other luminescence manifestations of the EHL can be found in the monograph [17].

8.4.2 Identification of the EHL emission band

Now we can summarize the typical spectral features that differentiate EHL luminescence from plenty of other lines or bands in the emission spectrum:

1. With increasing excitation intensity (even over several orders of magnitude) the EHL band firmly keeps its shape and position, i.e. neither band broadening nor a spectral shift occurs. This is due to the fact that the liquid density n_0 is constant at a given temperature (Fig. 8.9). An increase in the

[7] Also E'_g and E'_X are dependent on temperature but this dependence is weak in comparison with the temperature dependencies $F_e(T)$, $F_h(T)$ and $\mu'(T)$.

pump power density entails—no doubt—an increase in the total volume occupied by the drops and thus naturally also an increase in the emission intensity I^{EHL}, but the relevant spectral shape, driven by the density n_0, does not vary.

2. With increasing temperature two contradictory effects happen: the high-energy edge broadens (because more and more electrons and holes are excited above the respective Fermi levels), but, at the same time, the FWHM of the band gets slightly narrower (because the liquid density with increasing temperature drops slightly due to thermal expansion—see the liquid boundary of the phase diagram in Fig. 8.9). Consequently, the chemical potential $\mu'(T) = E'_g + F_e(T) + F_h(T)$ is a decreasing function of T, or $\varphi(T)$ becomes, according to (8.29), an increasing function of temperature; it turns out that this function can be written as

$$\varphi(T) = \varphi(0) + a(k_B T)^2,$$

where a is a constant of the order of 1 meV^{-1}.

3. The EHL phase diagram implies the existence of two distinct thresholds connected with EHL luminescence. The EHL band appears in the emission spectrum upon reaching an *intensity threshold*, which is nicely demonstrated in Fig. 8.13 [18]. On the other hand, the EHL band disappears

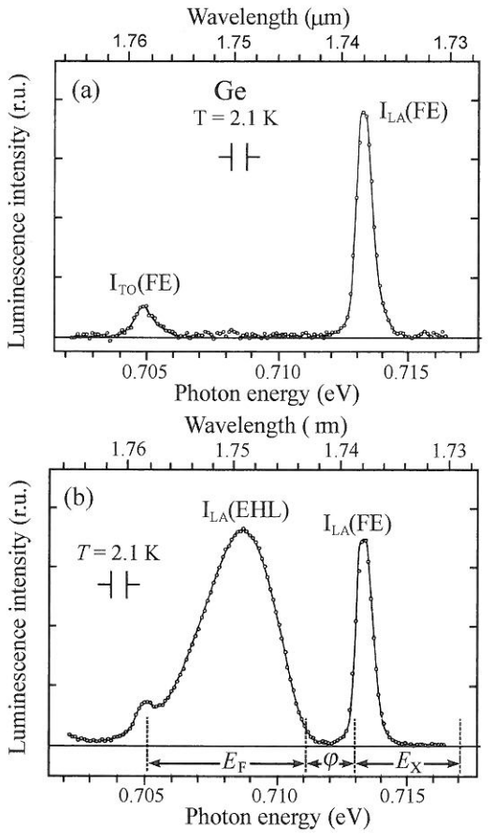

Fig. 8.13
Emission spectrum of ultrapure Ge at $T = 2.1\,\mathrm{K}$ under excitation with a tungsten lamp. (a) Excitation intensity is below the threshold for exciton condensation into the EHL. Only LA- and TO- phonon replicas of the free exciton are present. (b) Excitation intensity has been 2.2× increased. Suddenly the EHL band (LA-replica) at ~ 708.5 meV appears. After Westervelt [18].

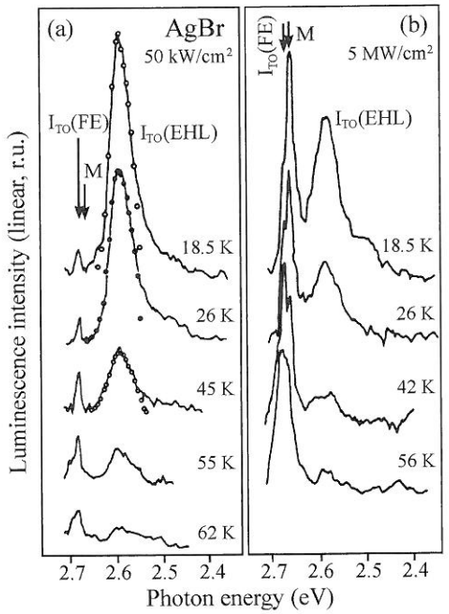

Fig. 8.14
Fast component of AgBr luminescence under pulsed laser excitation (380 nm, 6 ns). (a) Excitation intensity 50 kW/cm^2. Only the I_{TO}(EHL) band and a weak free exciton line I_{TO}(FE) occur. (b) Excitation intensity of 5 MW/cm^2. This high excitation induces, apart from the I_{TO}(EHL) and I_{TO}(FE) lines, also a very strong M-line due to excitonic molecules. Bath temperatures are indicated. The critical bath temperature is $T_c \sim 60$ K, which corresponds to the effective critical temperature of the *e–h* system of about 120 K. Symbols denote the theoretical shape (8.25) for $n_0 = 8 \times 10^{18}$ cm^{-3}. The intensity scales in (a) and (b) are not comparable. After Hulin *et al.* [19].

sharply upon reaching a *temperature threshold* (the critical temperature T_c), as can be seen in Fig. 8.14 [19]. The occurrence of both thresholds follows also from a simple kinetic model of nucleation and decay of electron–hole drops, see Appendix D.

The salient features (1.–3.) are very characteristic and enable one, as a rule, to make a facile identification of the EHL luminescence. Moreover, the considerable bandwidth of the EHL luminescence compared with, e.g., exciton lines may serve as primary guidance (see Fig. 1.1 where the replicas $I_{LO,TO}$(EHL) and I_{TA}(EHL) in silicon contrast with the narrow lines of free, FE, and bound, BE, excitons).

On the other hand, neither the analysis of the luminescence decay curves nor the shape of the intensity dependence of the EHL band is a reliable guide in this case. EHL luminescence decays faster than the free exciton emission (owing to Auger recombination in drops), but the shape of the decay curves as well as that of the intensity dependence may be strongly affected by the presence of parallel recombination processes (EM, BE, etc.).

8.4.3 Coexistence of excitonic molecules with electron–hole liquid

We have seen that under strong excitation various exciton interactions take place, among which especially EM and EHL affect significantly the low-temperature emission spectrum. Let us now ask whether in a semiconductor both the condensation of excitons into an EHL and the fusion of excitons into an excitonic molecule can occur simultaneously, or whether these are two

'disjunctive' processes in the sense that in a given material these may exist—depending upon the specific band structure—always just one of them.[8]

The attentive reader already knows the answer, of course. Comparison of Tables 8.1 and 8.2 shows that in AgBr, Si and Ge simultaneously $E_B > 0$ and $\varphi > 0$ hold, hence the gas of excitonic molecules can indeed coexist with the electron–hole liquid, In spite of this, there are certain points here—firstly, the remarkable historical context (the interpretation of the first luminescence experiments in highly excited Si and Ge crystals in the 1960s and 1970s oscillated between the EHL and EM models, because the correct answer to the above question was not known) and, secondly, interesting experimental aspects—which are worth mentioning.

Figure 8.14 compares AgBr emission spectra under a relatively low pulsed photoexcitation (50 kW/cm^2, panel (a)) with those taken with the excitation power density two orders of magnitude higher (5 MW/cm^2, panel (b)). Somewhat surprising is the occurrence of the M-line at the higher excitation only, while the EHL band is present in both these cases. It follows from these observations that, firstly, the equilibrium between the biexciton gas and the EHL (and, possibly, also the FE gas) may be limited to only a certain part of the phase diagram in the (n, T) plane, the so-called *biexciton pocket* [19]. Secondly, it turns out that the exciton condensation into an EHL is not entirely a typical 'high excitation effect'; a comparable, or perhaps an even more important role is played by a sufficiently low temperature. Condensation may often be achieved by making use of cw incandescent lamp excitation (see, e.g., Fig 8.13).

In Ge and Si the biexciton binding energy E_B is very small, not only in comparison with φ, but also absolutely. Consequently, at sufficiently low temperatures excitons very willingly condense into an EHL and thus the M-line cannot be observed at all, see Figs 1.1, 8.12 or 8.13. This is because the density of the surrounding free exciton gas, n_X, is low and biexcitons cannot form. If we simply decide to heat the sample in order to increase n_X and thus create biexcitons (which was realized in AgBr through heating the *e–h* system with powerful laser pulses, see Fig. 8.14(b)), we shall be faced with a problem. It is true that upon increasing the temperature by a couple of degrees we shall 'evaporate' more excitons, but at the same time we might already prevent biexciton formation because $k_B T \approx E_B$ will hold. Ultimately, at $T > T_c$ we shall dissolve the EHL entirely. Such a straightforward route cannot be applied, therefore the issue of the coexistence of EM with EHL remained unresolved for a long time.

We have to make the conditions for exciton condensation difficult, i.e. to make the EHL less stable, e.g. via stressing a Si sample along the [100] direction. In this way we lower the crystal symmetry and reduce the number of equivalent conduction band valleys ν_c from six to two. Therefore—according to what has been outlined above—we reduce the condensate binding energy φ. This means that the exciton gas surrounding the EHL drops gets denser, biexcitons can thus be created and, in the luminescence, the M-line appears. This is documented in Fig. 8.15 [20].

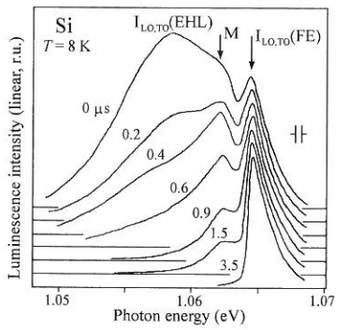

Fig. 8.15
Time-resolved emission spectra of a pure Si crystal, stressed along [100] at $T = 8$ K. Numbers at the curves indicate delay times (μs) after the excitation pulse. Besides the coexistence of all three phases—EHL, gas of FE and gas of EM—the figure also demonstrates the very rapid decay of the EHL luminescence. After Kulakovskii and Timofeev [20].

[8] With regard to what has been outlined in the introduction to Section 8.4, this inquiry concerns indirect-bandgap semiconductors.

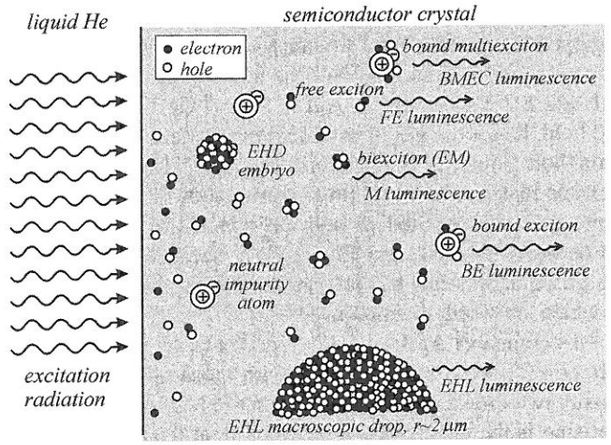

Fig. 8.16
Schematic cross-section of a (indirect-bandgap) semiconductor sample excited by light at low temperatures. Various luminescence processes are shown. After Westervelt [18].

An illustration of several parallel luminescence channels in semiconductors is given in Fig. 8.16. Let us add that, by using a special luminescence technique, the coexistence of an EHL with *free polyexcitons* (apart from biexcitons, with triexcitons and tetraexcitons) has been observed, particularly in silicon [21].

8.5 Electron–hole plasma (EHP)

8.5.1 Mott transition

Let us disregard for a moment the fact that the condensation of excitons can give rise to EHL drops. We thus have a gas of free excitons, the density of which, n_X, is continuously increased through the enhancement of excitation intensity. At the same time we also increase the number of free electron–hole pairs N, for a certain number of excitons always become ionized, even at low temperatures. In this way we reach a density N_M at which excitons as bound e–h pairs cease to exist. The reason for this resides in the effective screening of the Coulomb interaction between electrons and holes owing to the surrounding free carriers;[9] instead of (7.1), the interaction potential becomes

$$U_s(r) = -\frac{e^2}{4\pi\varepsilon_0\varepsilon r}\exp(-k_s r), \tag{8.30}$$

where $k_s = k_s(N) > 0$ is the so-called screening factor. Alternatively, $\lambda_s = k_s^{-1}$ is called the screening length. Relation (8.30) is known, e.g., from plasma physics.

The screening length $\lambda_s(N)$ gets shorter with increasing e–h pair density N. When λ_s approaches the free exciton radius a_X, excitons become unstable—the attraction between the electron and the hole is destroyed. As a first consequence of the screening (8.30), therefore, the transition of the exciton gas

[9] The proximity of other excitons operates in the same sense but it is commonly accepted that the main contribution to the screening comes from free electrons and holes.

(composed of bosons) through ionization to an *electron–hole plasma* (EHP) of a metallic character (i.e. driven by Fermi statistics) appears. This process represents one of a variety of possible realizations of the so-called *Mott insulator–metal transition*. The relevant density N_M is called the Mott density.

Bandgap renormalization arises as a second consequence. We have to realize that now we are far beyond the one-electron approximation. Due to Coulomb correlation and exchange effects, at high density of electron–hole pairs/excitons the semiconductor bandgap reduces to $E'_g(N) < E_g$. This can be demonstrated via a simple calculation, which compares the self-energy of a point charge in a many-electron system with that derived in the one-electron approximation [22]

$$\begin{aligned}\Delta E_g(N) = E'_g(N) - E_g &= \lim_{r\to 0}[U_s(r) - U(r)] \\ &= \frac{e^2}{4\pi\varepsilon_0\varepsilon}\lim_{r\to 0}\left[\frac{\exp(-k_s r) - 1}{r}\right] \\ &= \frac{e^2}{4\pi\varepsilon_0\varepsilon}\lim_{r\to 0}\left[-k_s\exp(-k_s r)\right] = -\frac{e^2}{4\pi\varepsilon_0\varepsilon}k_s(N) < 0,\end{aligned} \tag{8.31}$$

where we have used l'Hospital's rule. It follows immediately that $E'_g(N) < E_g$; the renormalization therefore entails a reduction of the bandgap ('gap shrinkage') in a dense electron–hole ensemble compared to the one-electron value E_g.

The Mott transition in an excitonic system is displayed schematically in Fig. 8.17. Already at densities N smaller than N_M by two orders of magnitude the value E_g begins to drop; at the Mott density N_M the curves $E'_g(N)$ and the ground exciton level $n = 1$ cross each other, which means that $E'_g(N) < E_g(0) - E_X$ for $N > N_M$. In other words, for the e–h system it becomes energetically more favourable to be in the continuum of states of free e–h pairs than to be bound into excitons. It might seem strange that the exciton $n = 1$ level is independent of N. In fact, however, this indicates that the binding energy E_X also drops with increasing N (due to screening) and this drop in E_X is just compensated by the drop in $E'_g(N)$. This information is very important because it tells us that the Mott transition to EHP is—unlike EHL nucleation—gradual, i.e. excitons do not disappear suddenly upon reaching N_M, but their concentration decreases slowly as a function of the increasing excitation intensity.[10]

The Mott density N_M can be calculated within various approximations. The calculation is fairly easy to perform considering a non-degenerate EHP with relevant Fermi distribution functions approximated by Boltzmann tails. The screening length λ_s is then called the *Debye–Hückel* screening length and one gets

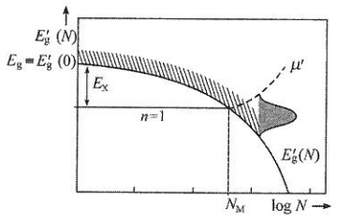

Fig. 8.17
The renormalized bandgap E'_g as a function of the e–h pair density N. The exciton binding energy of the $n = 1$ state is denoted E_X. The transition from the dielectric free exciton gas to ionized plasma EHP, proceeds smoothly. The EHP luminescence spectrum is depicted on the right; μ' stands for the plasma chemical potential, N_M is the Mott density.

[10] Gap shrinkage and the corresponding loss of excitonic resonances entail important qualitative changes in the optical absorption spectrum. Their features are obviously dependent on the excitation intensity and thus these spectral modifications represent a typical example of nonlinear optical phenomena.

$$\lambda_s \sim N^{-1/2},\ N_M \approx \frac{k_B T}{8\pi a_X^3 E_X} = \frac{k_B T\, \varepsilon_0\, \varepsilon}{e^2 a_X^2}. \qquad (8.32)$$

The Debye–Hückel model happens to be a viable approximation in semiconductors with large a_X, except at low temperatures. The temperature T in (8.32) may designate the effective temperature.

8.5.2 Luminescence of EHP

Electrons and holes in an EHP can recombine radiatively, of course. We are interested in what the EHP luminescence emission spectrum looks like. To begin, however, we have to answer an important question: What is the difference between an electron–hole plasma, EHP, and an electron–hole liquid, EHL, the existence of the latter having been—for the sake of simplicity—disregarded at the beginning of this section?

EHL and EHP are two similar phases of the e–h system. However, while the condensation exciton gas → EHL starts abruptly and the liquid is concentrated into spatially clearly separated regions—spherical drops with a constant e–h pair density n_0, the transition exciton gas → EHP proceeds smoothly, continuously. Also, the plasma gradually fills the whole excited volume (there are no drops) and may diffuse both laterally and into the depth of the sample, due to the concentration gradient. The e–h pair density therefore is not, unlike EHL, spatially constant and, moreover, rises with increasing excitation intensity. And perhaps the most important: the EHP may exist—unlike EHL—at arbitrary temperatures, neither is there an EHP critical temperature nor binding energy.

The EHP is therefore a 'less ordered' relative of EHL. There is no radiative recombination enhancement factor in EHP, unlike EHL. It is worth stressing, however, that the concept of the renormalized gap, as introduced in Subsection 8.4.1, holds equally for both EHP and EHL! If condensation into an EHL happens, the e–h system simply 'jumps' somewhere to the right in Fig. 8.17, far beyond the N_M density, and remains there. Equally, we can imagine that Fig. 8.11 is valid for both EHL and EHP, but while $E'_g(n_0)$ is constant inside EHL drops, $E'_g(N)$ in EHP varies as a function of N (see Fig. 8.17).

The scenario under growing optical excitation intensity, e.g., in silicon at $T = 15\,\mathrm{K}$, can then be described as follows (see the horizontal arrow in Fig. 8.9): First, a gas of excitons with increasing density n_X is created, but before the Mott transition sets in, n_X reaches a critical value for exciton condensation into EHL drops with a very high equlibrilum e–h pair density $N = n_0 \approx 3 \times 10^{18}\,\mathrm{cm}^{-3}$. The density of the surrounding gas, n_X, henceforth remains constant[11] ($\sim 10^{16}\,\mathrm{cm}^{-3}$) and the gradual Mott transition will not occur. Generally it turns out that in indirect-bandgap materials, EHP and its luminescence reveal themselves only at temperatures $T = T_c$ or higher. To differentiate the contributions to the emission spectrum from EHL, EHP and possibly from other luminescence channels (biexcitons, etc.) under these

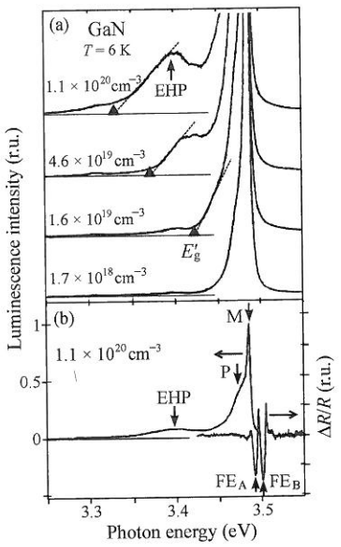

Fig. 8.18
(a). Onset of the EHP emission band in highly excited GaN at $T = 6\,\mathrm{K}$ upon reaching the Mott density ($N_M \approx 10^{19}\,\mathrm{cm}^{-3}$). Triangles label the positions of the reduced bandgap E'_g at the indicated densities of e–h pairs. Panel (b) displays the overall shape of the emission spectrum. Apart from the EHP band, also the M-line due to biexciton luminescence and the P-line due to exciton collisions are present. The free exciton spectral position is given by the reflection spectrum $\Delta R/R$. After Nagai *et al.* [23].

[11] The average density of the e–h system (all phases) will rise with the continuing growth of the excitation level, though, due to the growth the total volume of the EHL drops.

conditions is not easy. Some authors even take the view that EHP can also undergo its own condensation process, characterized by a second critical point in the phase diagram. Currently, there is no consensus on this issue and further discussion goes beyond the scope of this book.

In this respect, the situation is much simpler in direct-bandgap semiconductors, where EHL does not occur. The onset of EHP luminescence under sufficiently strong excitation is straightforward there, and according to the foregoing discussion this light emission has very specific spectral features:

1. A wide emission band (much like an EHL—radiative recombination in an ensemble of fermions), gradually emerging in the spectrum when the density of e–h pairs, N, approaches N_M.
2. The low-energy emission band boundary (determined by $E'_g(N)$) undergoes a red shift with increasing excitation intensity; for an EHL, this boundary does not shift.
3. With increasing excitation intensity the EHP emission band gets broader, because the plasma density increases; the EHL bandwidth remains fixed.

Examples are shown in Figs 8.18 (GaN [23]) and 8.19 (TlBr [24]). The gradual increase of the EHP band around $N = N_M$—the salient feature (1)—can be nicely seen in Fig. 8.18, while Fig. 8.19 demonstrates features (2) and (3).[12] Open circles in Fig. 8.19 represent a theoretical fit from which the displayed EHP densities were derived.

It is important to stress that, although in TlBr the direct bandgap is concerned here, expression (8.25) together with the procedure described in Subsection 8.4.1 were applied for fitting. This is surprising because the convolution (8.25) was derived for an indirect bandgap. Here, strictly speaking, its application is not justified. Nevertheless, this phenomenological approach is currently being used because it is simple and provides us with both a reasonable reproduction of the emission bandshape and a realistic effective temperature and density of EHP. (This was one of the reasons to depict transitions in Fig. 8.11 as direct ones.) More elaborate routines for spectral modelling that comprise **k**-*conservation* have been proposed, of course, but they are rather sophisticated and the resulting spectral shape is almost the same, except for more accurate determination of E'_g [25].

Let us recall once more that the densities obtained through fitting are *average* EHP densities, unless we create in some way a spatially uniform plasma which, in fact, is highly desirable for the comparison of theory with experiment. To this end for example, two-photon excitation discussed in Section 5.5 can be used, as well as various spatial localizations of EHP in low-dimensional structures. Finally, let us note that radiative recombination of EHP in direct semiconductors may easily lead to stimulated emission (Chapter 10), which is of basic importance for light-emitting diodes and semiconductor lasers.

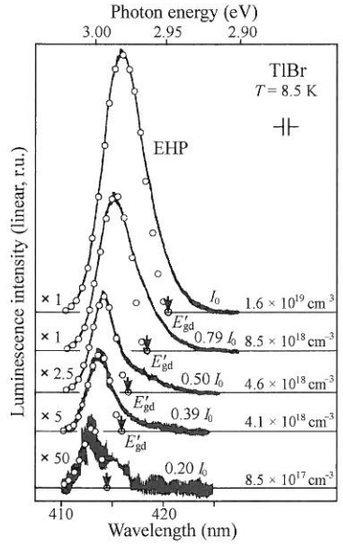

Fig. 8.19
EHP emission spectra in a highly excited TlBr crystal (a pulsed N_2-laser, 2 ns, 3.4 eV) at a bath temperature of 8.5 K. The excitation intensity I_0 corresponds to $\sim 0.6\,\mathrm{MW/cm^2}$. In TlBr, radiative recombination can occur both in indirect as well as in direct bandgaps; the displayed spectra originate in the direct one, whose reduced values E'_{gd} are labelled by arrows. After Kohlová *et al.* [24]. (Fig. 2.38(b) represents the EHP emission spectrum of TlBr at $T = 25\,\mathrm{K}$ both in direct—A-line—and indirect—B-line—bandgaps. Arrows at $\sim 3.02\,\mathrm{eV}$ and $\sim 2.66\,\mathrm{eV}$ denote the spectral positions of relevant non-renormalized gaps corresponding to the one-electron approximation. The respective plasma densities and effective temperatures are also shown.)

[12] Let the reader compare Fig. 8.19 with Fig. 8.14, where the I_{TO}(EHL) spectral position remains fixed in spite of the variation in excitation power density by two orders of magnitude.

8.6 Bose–Einstein condensation of excitons

An exciton as a quasi-particle consisting of two fermions (an electron and a hole) always has an integer total spin $S = 0$ or 1. An exciton is thus a boson and these can undergo, at high densities, so-called Bose–Einstein condensation. It is worth stressing that Bose–Einstein condensation represents a fundamentally different process with regard to exciton condensation into an EHL discussed above. In order to understand the fundamentals of Bose–Einstein condensation and to discover how this kind of exciton condensation can manifest itself in luminescence, we first recall the basic properties of Bose–Einstein statistics.

8.6.1 Properties of the Bose–Einstein distribution

The distribution or occupation function of ideal (non-interacting) bosons, determining the mean boson' number in a state with energy E, reads

$$f_{\mathrm{BE}}(E,T) = \frac{1}{\exp\left(\frac{E-\mu}{k_{\mathrm{B}}T}\right) - 1}, \tag{8.33}$$

where μ is the chemical potential. This function is called the Bose–Einstein distribution. Unlike the Fermi–Dirac distribution, where μ is more often known as the Fermi energy and has quite an illustrative meaning of an energy level with the occupation probability equal to 1/2, the chemical potential μ in (8.33) is less familiar. Its properties are:

1. $\mu < 0$ must be satisfied, otherwise the distribution function (8.33) in the ground state ($E = 0$) would acquire a negative value, which is not admissible.
2. $|\mu|$ is large at low boson densities, while with increasing density $|\mu|$ decreases and gradually approaches zero. This also follows directly from (8.33); a large value of $|\mu|$ implies a low mean number of bosons in a given state.

Let us now ask a question: Can the boson' number in the investigated system reach an arbitrary value? The total boson' number (per unit volume) n_{tot} can be found by summing over all occupied states and all possible energies:

$$n_{\mathrm{tot}} = \int_0^\infty \rho(E) f_{\mathrm{BE}}(E)\, \mathrm{d}E. \tag{8.34}$$

For bosons with a mass m and total spin $S = 0$ we shall consider the density of states of the form[13] $\rho(E) = (2m)^{3/2}E^{1/2}/4\pi^2\hbar^3$. The maximum available number of bosons, n_{CB}, can be obtained if we introduce into (8.34) a maximum value of f_{BE}, which, according to the foregoing discussion, occurs in the limiting case $\mu \to 0$. By performing the relevant calculation (Appendix E) we get

[13] The difference 1/2 compared to (5.4) is due to the difference in the spin degeneracy factor g between fermions ($g = 2$) and bosons with spin $S = 0 (g = 1)$.

$$n_{\mathrm{CB}}(T) = \frac{2.31\ (2m)^{3/2}\,(k_{\mathrm{B}}T)^{3/2}}{4\pi^2\hbar^3}$$

$$\cong 2.61\left(\frac{m\,k_{\mathrm{B}}T}{2\pi\hbar^2}\right)^{3/2} \cong 6.4\times 10^{15}\left(\frac{m}{m_0}\right)^{3/2} T^{3/2}(\mathrm{cm}^{-3}), \tag{8.35}$$

where m_0 stands for the free electron mass. Obviously, this is a finite number, thus a very important message from (8.35) is: an ensemble of bosons may always contain only a *finite* number of particles (dependent on temperature).

What happens now if we continuously add further particles into the ensemble? (In particular, if we keep creating a higher and higher exciton density through increasing the optical excitation?)

Einstein, shortly after the formulation of quantum statistics by the Indian physicist Bose, deduced: the excess particles must 'condense' to the ground state $E = 0$, which, in this way, somehow separates from other states. Relation (8.35) thus defines a *critical concentration* n_{CB} for the onset of this so-called Bose–Einstein condensation,[14] which occurs primarily in energy or momentum space (**k**-space), not in real space—unlike exciton condensation to an EHL.

Before we discuss manifestation of luminescence the of this peculiar condensation, we shall derive one simple mathematical consequence of (8.35). Upon reaching n_{CB} we can obviously express the boson density as

$$n_{\mathrm{tot}} = n_0 + n_{\mathrm{CB}}(T).$$

The ground state population n_0 will thus grow with a further increase of pumping, while n_{CB} at a given T remains constant. This relation can be rewritten as

$$\frac{n_0}{n_{\mathrm{tot}}} = 1 - \frac{n_{\mathrm{CB}}}{n_{\mathrm{tot}}} = 1 - \frac{6.4\times 10^{15}\ (m/m_0)^{3/2}\ T^{3/2}}{n_{\mathrm{tot}}},$$

from which the *critical temperature* T_{CB} for the Bose–Einstein condensation can be defined via

$$\frac{1}{T_{\mathrm{CB}}^{3/2}} = \frac{6.4\times 10^{15}\ (m/m_0)^{3/2}}{n_{\mathrm{tot}}}. \tag{8.36}$$

The announced mathematical follow-up of (8.35) then reads

$$\frac{n_0}{n_{\mathrm{tot}}} = 1 - \left(\frac{T}{T_{\mathrm{CB}}}\right)^{3/2}. \tag{8.37}$$

From (8.37) we can easily infer the meaning of the critical temperature:

For $T > T_{\mathrm{CB}}$ ..... (8.37) has no physical meaning,
$T = T_{\mathrm{CB}}$ ..... $n_0 = 0$ and the condensation just begins,

[14] At the same time a condition must be satisfied, namely, that the energy and the number of bosons can vary independently. This is possible, e.g., for atoms, excitons and biexcitons but not for photons and phonons; their chemical potential equals zero but, despite this fact, one cannot speak of a Bose–Einstein condensation. An equivalent statement reads that bosons undergoing Bose–Einstein condensation must have non-zero rest mass (see (8.35)), which holds neither for photons nor phonons.

$T < T_{CB}$ ..... n_0 according (8.37) sharply increases,
$T = 0\,K$ ..... $n_{tot} = n_0$.

On the basis of (8.36) and (8.37) we can quite clearly imagine what the Bose–Einstein condensation of excitons looks like in an experiment. Let us apply, e.g., a fixed excitation intensity, i.e. a fixed exciton density $n_X = n_{tot}$, and let us start the experiment at a relatively high temperature when, according to (8.35), $n_X < n_{CB}(T)$. Therefore there is no condensation. In the course of cooling we reduce $n_{CB}(T)$ till we drop to the critical temperature T_{CB} when $n_X = n_{CB}$. The condensation sets in and if we keep cooling, the concentration of 'condensed' excitons rises according to (8.37) up to the limit value $n_0 = n_X$ at $T = 0\,K$. Then, all of the photogenerated excitons occur in the condensate with energy $E = 0$.

8.6.2 Luminescence experiment: Bose–Einstein condensation yes or no?

The Bose–Einstein condensation represents the macroscopic population of a single state $E = 0$ or $\mathbf{k} = 0$. It is one of the fundamental consequences of quantum mechanics that leads—among others—to important, application-related effects like superfluidity of liquid He and superconductivity. The development of efficient laser and magnetic cooling of atoms has recently led to a fruitful investigation of experimental features of this condensation in an atomic gas, but at extremely low temperatures below 100 nK.

Semiconductor luminescence proposes unique conditions for a detailed study of Bose–Einstein condensation. If we adjust (8.36) to express explicitly the critical temperatures

$$T_{CB} \cong 2.9 \times 10^{-11} \left(\frac{m_0}{m}\right) n_{tot}^{2/3}\,(K), \tag{8.38}$$

it is observed that the critical temperature for an atomic gas ($m \gg m_0$) is by many orders lower compared with a gas of excitons ($m \approx m_0$) of the same density. Considering this density to be $n_{tot} = 10^{17}\,cm^{-3}$ (easily attainable under optical pumping), we obtain from (8.38) for $m = m_0$ a critical temperature $T_{CB} \approx 6.3\,K$. This is a 'reasonable' temperature that can be achieved in a current helium cryostat. Pumping of ^{4}He vapour enables going down to $T \approx 1.3\,K$ commonly. There are additional advantages: the exciton density and thus, according to (8.38), also T_{CB} can be varied readily via the variation of excitation intensity, or vice versa, at a given excitation power density we can finely tune the sample temperature in the environs of T_{CB}. And, most importantly, the exciton condensate reveals itself through a dramatic modification of the semiconductor emission spectrum. For all of these reasons the search for the Bose–Einstein condensation of excitons using luminescence methods has represented a worldwide challenge for more than 30 years.

How the condensation should manifest itself in the emission spectrum can be predicted first with the aid of simple reasoning. Since it arises from the accumulation of excitons in the $E = 0$ state, which corresponds to the bottom of the exciton band, we expect the recombining 'condensed' excitons to emit

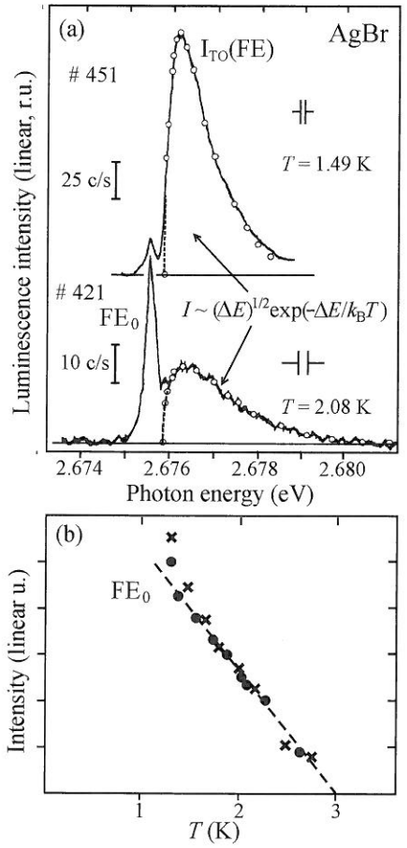

Fig. 8.20
(a) Low-temperature free exciton photoluminescence in AgBr accompanied with the emission of a TO(L)-phonon (i.e. I_{TO}(FE) line), in two samples #451 and #421. Open circles denote the theoretical lineshape fit based on (7.16). The very narrow peak labelled FE_0 has been identified as being due to the Bose–Einstein condensation of the free exciton gas. Panel (b) shows a sudden intensity increase of this peak in the course of cooling below 3 K. After Czaja and Schwerdtfeger [26]. Later experiments revealed that this interpretation was probably incorrect, though.

a very narrow peak on the low-energy edge of the free exciton line ($h\nu = E_{gi} - E_X - \hbar\omega$ in an indirect-bandgap semiconductor). This peak should appear in the spectrum suddenly in the course of cooling, upon reaching T_{CB}.

Exactly this kind of behaviour can be recognized in the spectra shown in Fig. 8.20(a), which come from two nominally pure AgBr crystals at $T = 2.08\,K$ and $T = 1.49\,K$. The lower panel (b) shows that the intensity behaviour of the sharp FE_0 peak at $\sim 2.6754\,eV$ complies perfectly with (8.37), provided we put $T_{CB} = 3\,K$. This represents one of the first luminescence observations interpreted in terms of the excitonic Bose–Einstein condensation [26]. Everything looks very convincing. However, a series of subsequent papers revealed this interpretation to be untenable, by finding the origin of the FE_0 peak in an exciton bound to a residual shallow impurity (Subsection 7.2.1).

This indicates that the experimental realization of the Bose–Einstein exciton condensation is not a simple task and that such a straightforward way as the one shown in Fig. 8.20 is hardly viable. A 'jump' from the Maxwell–Boltzmann distribution (circles on the experimental curves in Fig. 8.20(a)) immediately to the spectrally narrow condensate is unrealistic. The Maxwell–Boltzmann distribution is a classical limit, shared both by bosons and fermions. With

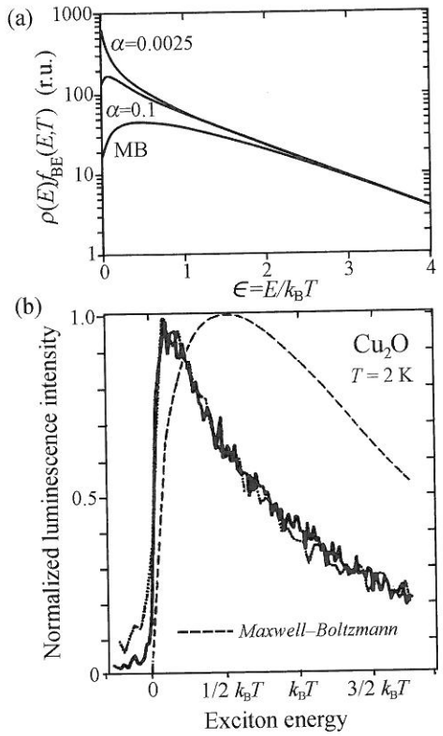

Fig. 8.21
(a) Product of the density of states $\rho(E) \approx \sqrt{E}$ with the Bose–Einstein distribution function (8.33) where $\alpha = -\mu/k_BT$. The lower curve (MB) is the Maxwell–Boltzmann approximation valid for low exciton densities ($\alpha > 4$). In the limit $\alpha \to 0$ a narrow peak remains only at $\epsilon = 0$. The curves are normalized at high values of ϵ. (b) Narrowing down of the exciton emission line (a phonon replica) in Cu_2O at high exciton density. The sample was immersed in liquid He ($T = 2$K) and excited by 10 ns pulses of an Ar^+-laser with excitation intensity of $\sim 40\,MW/cm^2$. The dashed curve (Maxwell–Boltzmann distribution) is considerably wider. After Snoke *et al.* [27].

increasing density n_X (therefore with decreasing $|\mu|$) the excitons should at first prove that they start to behave as genuine bosons. Consequently, the exciton statistics and also the emission lineshape should gradually transform to true Bose statistics. In this case, the lineshape width would undergo dramatic but gradual narrowing, which can be easily shown by calculating $\rho(E)\,f_{BE}(E)$ and which is displayed in Fig. 8.21(a). This is the so-called *Bose narrowing*. The reader is reminded that the FWHM of the Maxwell–Boltzmann distribution (7.16) is invariable, equal to about $1.8\,k_BT$.

This Bose narrowing has indeed been found in exciton luminescence of Cu_2O [27], as demonstrated in Fig. 8.21(b). Nevertheless, till now, no unambiguous experimental evidence of Bose–Einstein condensation has been achieved either in this material or in bulk semiconductors in general (at least unconditional evidence that would be accepted without taking exceptions to). Taking into consideration everything discussed above in this chapter, we understand why this is so. First of all, excitons have a finite lifetime. The ideal Bose–Einstein distribution (8.33) holds exactly for excitons as non-interacting quasiparticles with infinite lifetime in thermodynamic equilibrium only. Moreover, with increasing exciton density the important exciton–exciton interactions occur in most semiconductors (biexcitons, EHL, EHP). For instance, prior to reaching the critical concentration n_{CB}, the Coulomb e–h attraction may happen to be screened and the exciton gas transformed into EHP or EHL. (This is one of the reasons why especially Cu_2O appears to be a good candidate

for the exciton Bose–Einstein condensation—owing to specific features of the Cu_2O band structure the interaction between excitons is repulsive, thus biexcitons do not originate here. Moreover, because the Bohr radius a_X is very small, see Table. 7.1, EHP does not occur in this material at high excitation.)

Another complication preventing excitons from Bose–Einstein condensation may be insufficient sample purity, as we have seen in the case of AgBr (Fig. 8.20)—the presence of bound excitons reduces n_X and, in the spectrum, may either mask a possible emission line arising from the Bose–Einstein condensate or cause an incorrect interpretation of the experimental observations. Finally, high optical excitation levels can both evoke spatial exciton diffusion and entail a high effective temperature of the exciton gas that hinders reaching T_{CB}. A more detailed discussion goes beyond scope of this book. It is worth mentioning though, that also biexcitons are bosons and one can expect their Bose–Einstein condensation together with its specific luminescence manifestation. The most investigated material in this regard is copper chloride, CuCl. The whole topic is covered by a special monograph [28].

It is worth noting that, strictly speaking, the above discussed 'classical' Bose–Einstein condensation may exist in infinite bulk materials only. In low-dimensional systems, a generalized definition of Bose–Einstein should be applied. In particular in two-dimensional structures the concept of condensation is linked to the phase-coherent superfluid movement of a bosonic system rather than to boson accumulation in the lowest energy level [29]. Recent results concerning Bose–Einstein condensation of exciton–polaritons in semiconductor low-dimensional microcavities will be briefly mentioned in Chapter 16.

8.7 Problems

8/1: Based on Fig. 8.1: (a) Estimate the binding energy E_B of an excitonic molecule in CdS. (b) Check that the spectral position of the P-band, which is due to inelastic exciton–exciton scattering, is in accord with the binding energy E_X in Table 7.1.

8/2: Luminescence of excitonic molecules in indirect-bandgap semiconductors, discussed in Subsection 8.2.1, has been described in the framework of allowed dipole transitions. Nakahara and Kobayashi [30] have generalized this approach for the case of *indirect forbidden* transitions, when the relevant transition matrix element is composed of two terms, the first of which is proportional to the magnitude of the biexciton wavevector $\mathbf{Q}$ and the second one to the magnitude of the wavevector $\mathbf{q}$ of the remaining exciton. Making use of the formalism applied in Appendix C, adjust the expression describing the emission lineshape to a form suitable for numerical integration (analogy with (C-15)) and show that the contribution of the second term is negligible.

8/3: Prove, using the $E(\mathbf{K})$ diagram (in analogy with Fig. 8.7), that in common semiconductors with indirect bandgap the luminescence channel due to inelastic free exciton collisions (P-line) cannot occur. Hint: consider that the indirect bandgap in common semiconductors is always defined by an

extreme of the conduction or valence band situated at the boundary of the first Brillouin zone.

8/4: Show that the average kinetic energy (per electron) in a Fermi gas at $T = 0$ K is equal to $(3/5)F_e$ (F_e = Fermi energy of electrons).

8/5: An electron–hole liquid (EHL) in the form of electron–hole drops (EHDs) represents an open system exchanging quasi-particles, i.e. the electron–hole pairs, with its surroundings. Open systems in thermodynamics are characterized, among others, by their chemical potential μ. Show that here μ is characteristic of the EHL ground state. Hint: start from the definition of the chemical potential as the energy required for passing from the ground state with N electron–hole pairs in a drop to the ground state with $(N + 1)$ pairs in the drop. See also [31].

8/6: By using the relationship (8.32) and exploiting the parameters from Table. 7.1, calculate the Mott density N_M in selected semiconductors for $k_B T/E_X = 0.1$. Compare the obtained results with a rough estimate derived on the basis of the criterion $N_M \cong (4\pi a_X^3/3)^{-1}$. Discuss the illustrative meaning of this criterion.

References

1. Shionoya, S., Saito, H., Hanamura, E., and Akimoto, O. (1973), *Solid State Comm.*, **12**, 223.
2. Klingshirn, C. and Haug, H. (1981). *Phys. Rep.*, **70**, 315.
3. Hanamura, E., and Haug, H. (1977). *Phys. Rep., C*, **33**, 209.
4. Quattropani, A. and Forney, J. J. (1977). *Nuovo Cimento B*, **39**, 569.
5. Grun, J. B., Lévy, R., Ostertag, E., Vu Duy Phach, H., and Port, H. (1976). *Biexciton luminescence in CuCl and CuBr*. In: *Physics of Highly Excited States in Solids* (ed. M. Ueta and Y. Nishina), Lecture Notes in Physics Vol. 57, p. 49. Springer, Berlin.
6. Baba, T. and Masumi, T. (1977). *Nuovo Cimento B*, **39**, 609.
7. Cho, K. (1973). *Optics Comm.*, **8**, 412.
8. Knox, R. S., Nikitine, S., and Mysyrowicz, A. (1969). *Optics Comm.*, **1**, 19.
9. Pelant, I., Hála, J., Parma, L., and Vacek, K. (1980). *Solid State Comm.*, **36**, 729.
10. Gourley, P. L. and Wolfe, J. P. (1979). *Phys. Rev. B*, **20**, 3319.
11. Hvam, J. M. (1973). *Solid State Comm.*, **12**, 95.
12. Moriya, M. and Kushida, T. (1976). *J. Phys. Soc. Japan*, **40**, 1668.
13. Shah, J., Combescot, M., and Dayem, A. H. (1977). *Phys. Rev. Lett.*, **38**, 1497.
14. Rice, T. M. (1977). *The electron–hole liquid in semiconductors: theoretical aspects*. In: *The Electron–Hole Liquid in Semiconductors* (ed. H. Ehrenreich, F. Seitz and D. Turnbull), Solid State Physics Vol. 32, p. 1. Academic Press, New York.
15. Vashista, P., Kalia, R. K., and Singwi, K. S. (1983). *Electron–hole liquid: theory*. In: *Electron–Hole Droplets in Semiconductors* (ed. C. D. Jeffries and L. V. Keldysh), Modern Problems in Condensed Matter Sciences Vol. 6, p. 1. North Holland, Amsterdam.
16. Benoit à la Guillaume, C. and Voos, M. (1973). *Phys. Rev. B*, **7**, 1723.
17. Hensel, J. C., Phillips, T. G., and Thomas, G. A. (1977). *The electron–hole liquid in semiconductors: experimental aspects*. In: *The Electron–Hole Liquid in Semiconductors* (ed. H. Ehrenreich, F. Seitz and D. Turnbull), Solid State Physics Vol. 32, p. 88. Academic Press, New York.
18. Westervelt, R. M. (1983). *Kinetics of electron–hole drop formation and decay*. In: *Electron–Hole Droplets in Semiconductors* (ed. C. D. Jeffries and L. V. Keldysh), Modern Problems in Condensed Matter Sciences Vol. 6, p. 187. North Holland, Amsterdam.
19. Hulin, D., Mysyrowicz, A., Combescot, M., Pelant, I., and Benoit à la Guillaume, C. (1977). *Phys. Rev. Lett.*, **39**, 1169.
20. Kulakovskij, V. D. and Timofeev, V. B. (1983). *Thermodynamics of electron-hole liquid in semiconductors*. In: *Electron–Hole Droplets in Semiconductors* (ed. C. D. Jeffries and L. V. Keldysh), Modern Problems in Condensed Matter Sciences Vol. 6, p. 95. North Holland, Amsterdam.
21. Steele, A. G., McMullan, W. G., and Thewalt, M. L. W. (1987). *Phys. Rev. Lett.*, **59**, 2899.
22. Haug, H. (1988). *Introduction*. In: *Optical Nonlinearities and Instabilities in Semiconductors* (ed. H. Haug), p. 1. Academic Press, New York.
23. Nagai, T., Inagaki, T. J., and Kanemitsu, Y. (2004). *Appl. Phys. Lett.*, **84**, 1284.
24. Kohlová, V., Pelant, I., Hála, J., Ambrož, M., and Vacek, K. (1987). *Solid State Comm.*, **62**, 105.
25. Capizzi, M., Modesti, S., Frova, A., Staehli, J. L., Guzzi, M., and Logan, R. A. (1984). *Phys. Rev. B*, **29**, 2028.
26. Czaja, W. and Schwerdtfeger, C. F. (1974). *Solid State Comm.*, **15**, 87.
27. Snoke, D. W., Wolfe, J. P., and Mysyrowicz, A. (1990). *Phys. Rev. B*, **41**, 11171.
28. Moskalenko, S. A. and Snoke, D. W. (2000). *Bose–Einstein Condensation of Excitons and Biexcitons*. Cambridge University Press, Cambridge.
29. Kavokin, A. V., Baumberg, J. J., Malpuech, G., and Laussy F. P. (2007). *Microcavities*. Oxford University Press, Oxford.
30. Nakahara, J. and Kobayashi, K. (1976). *J. Phys. Soc. Japan*, **40**, 189.
31. Combescot, M. and Noziéres, P. (1972). *J. Phys. C*, **5**, 2369.